Controlling factors in tensile deformation of nanocrystalline cobalt and nickel

Y. M. Wang, R. T. Ott, T. van Buuren, T. M. Willey, M. M. Biener, and A. V. Hamza

Phys. Rev. B **85**, 014101 — Published 5 January 2012

DOI: 10.1103/PhysRevB.85.014101

Controlling factors in tensile deformation of nanocrystalline cobalt and nickel

Y.M. Wang[*, 1], R.T. Ott[2], T. van Buuren[1], T.M. Willey[1], M.M. Biener[1], A.V. Hamza[1]

[1]Physical and Life Sciences Directorate, Lawrence Livermore National Laboratory, Livermore, CA 94550, USA

[2]Division of Materials Science and Engineering, Ames Laboratory (USDOE), Ames, Iowa 50011, USA

Abstract

In an effort to understand and enhance the tensile ductility of truly nanocrystalline metals, we have investigated and compared the mechanical behavior, especially the tensile behavior, of hcp nanocrystalline cobalt (~20 nm) and fcc nanocrystalline nickel (~28 nm). Although both materials exhibit obvious plasticity in tension, their uniform tensile ductility, tensile elongation-to-failure, and fracture behavior are drastically different. In-situ synchrotron x-ray diffraction and ultra-small angle x-ray scattering reveal distinct deformation disparity in terms of residual strain development, texture evolution, nanovoid formation, and subsequent strain hardening and strain rate hardening behavior. The dependence of tensile property on the strain rate and temperature is examined and discussed. Factors that influence the strength and ductility of nanocrystalline metals are considered and prioritized according to the current findings. A new Hall-petch relationship is proposed for nanocrystalline nickel.

Keywords: nanocrystalline metals; tensile property; Hall-petch relationship; in-situ synchrotron x-ray diffraction; USAXS

PACS number(s): 62.20.M-, 81.07.Bc, 29.20dk, 61.05.cf

Contact email: ymwang@llnl.gov

I. INTRODUCTION

Tensile property of nanocrystalline (nc) metals (grain size d<100 nm) is arguably one of the most important variables to evaluate the potential utilities of these advanced materials.[1] Unfortunately, unlike other mechanical testing methods (e.g., uniaxial compression, nano- or micro-indentation, rolling), the uniaxial tensile testing is overwhelmingly sensitive to various extrinsic defects in nc materials such as nanovoids, impurities, residual stresses, and dogbone sample geometry and surface conditions.[2-4] Not surprisingly, the tensile property of many existing results in the literature cannot be directly compared, as those data were often acquired from various tensile samples with different geometries/sizes, synthesized and cut by different techniques, and/or tested by dissimilar loading frames. For instance, the tensile yield strength (σ_y) of nc nickel with an average d of 20 nm could vary from 0.81 GPa[5] to 1.60 GPa[2] even if the materials were all fabricated by pulsed electrodeposition (ED) method. The spread of data becomes even more problematic when the tensile elongation to failure (ε_{tef}) of nc materials is compared; e.g., for nc nickel with d~20-30 nm, the reported ε_{tef} value ranges as much as from 0.01 to 0.11.[2, 3, 5-7] These drastic variations of tensile properties, yet in a monolithic fcc nc metal such as nickel, not only make it difficult to substantiate computer models from experiments, but also strongly suggest that there remains a pressing need to investigate possible variables and mechanisms controlling the tensile property of nc materials. The tensile ductility (i.e., ε_{tef}) of nc metals, in particular, is poorly understood, as it is intricately related to the necking and fracture process of nc materials, and can hardly be addressed by a single existing model.

In addition to the astonishingly scattered tensile data, contradictive trends were reported on the strain-rate and temperature dependent tensile properties of nc metals. For example, Lu *et al.*[8] and Schwaiger *et al.*[7] observed that the tensile ductility increases with increasing strain rates in nc copper and nc nickel, respectively, whereas the opposite trend was witnessed by Dalla Torre *et al.*[2] and Karimpoor *et al.*[9] in nc nickel and nc cobalt, respectively. Although nc cobalt has an hcp structure and distinctive slip/twinning systems compared to fcc nc metals, the inconsistent trends seen in nc nickel itself cast serious doubts on whether the tensile ductility trend is correlated with the crystallographic structure of nc materials and/or their slip/twinning systems. A recent grain boundary (GB) affected zone model[7] has in fact suggested that GBs rather than the slip systems play more significant roles in deciding the tensile ductility trend of nc metals. This hypothesis can be expectedly true especially when d decreases below 30 nm

where GB activities become dominant, as suggested by numerous molecular dynamics (MD) simulations.[10] Experimentally, however, the existing evidence is inconsistent at best. The very limited results available on different crystallographic nc materials (with different slip/twinning systems) call for further critical research in this direction.

While sample size effect, porosities and flaws, and intrinsic deformation behavior have been invoked as possible explanations for the extremely large scatter in the tensile data, other important experimental aspects such as tensile sample cutting and preparation technique have not been investigated in the literature. In fact, almost all tensile data reported so far were measured using samples prepared by wire electro-discharging machining (EDM), the effect of which on tensile behavior was not documented. To extract the intrinsic tensile behavior of various nc metals and its influencing factors, it is obviously important and necessary that flaw-free nc samples are used. Such "ideal" nc materials, however, only exist in computer simulations. So far, ED is popularly considered as one of the most effective techniques to prepare nearly fully-dense nc metals and alloys. There are lingering issues, however, concerning the materials prepared via this route, including: (1) they are not impurity free. Some common contaminants such as sulfur have the tendency to segregate and have non-negligible impact on the mechanical behavior; (2) texture remains in ED-synthesized nc metals even though it is considered minor.[2, 9] The existence of texture suggests fiber or columnar grain structure, which could complicate the tensile property measurements, and thus, requires microstructure characterizations of ED samples on both cross-sectional and plan-view directions; and (3) the possible presence of cavities or nanopores inside grains, along GBs or triple junctions is not well portrayed.[11, 12] The existence of nanovoids, which could be connected with hydrogen co-deposition or the space left during the nanograin coalescence and growth,[13] is difficult to detect and prevent. If they exist, the impact of these nanovoids is a major concern and could alter the tensile property, i.e., render low strength and limited plastic deformation. Yet little work has been performed to investigate these nanovoids. The microstructure complexity of ED nc materials undoubtedly requires more thorough examinations of their tensile properties. To warrant that the experimental results are meaningful and comparable in different crystallographic nc materials, it is of paramount importance that the same sample dimensions, processing and cutting methods, and polishing conditions are used, and that all tensile property measurements are accompanied by careful documentations of microstructure, impurities, and voids.

In an effort to decode above inconsistencies in the literature and improve our current understanding on tensile ductility of nc materials, this work investigates the tensile behavior of two different crystallographic ED materials, i.e., nc cobalt (hexagonal close-packed, hcp) and nc nickel (face-centered cubic, fcc). With the exception of different crystallographic structures, these two elements have similar melting temperatures and other physical properties (see Table 1). Therefore, it is helpful to evaluate their temperature dependent deformation characteristics and the resultant tensile properties. Note that the actual aspects of tensile behavior in nc materials may depend upon various external parameters (e.g., deformation temperature and strain rate) and internal factors (e.g., composition, texture, crystal structure, and voids). The propensity for tensile failure and its correlation to strain hardening and strain rate sensitivity could be universal to various nc materials.[14-18] One key aim of this work is to uncover these underlying linkages by orchestrating findings among microstructure characteristics, materials deformation parameters, and macroscopic tensile behavior. We arrange this paper according to the following scheme. At the outset, we will carefully document the microstructure details and impurity levels of our nc materials with the emphasis on the complexity of initial microstructure and artifacts/flaws induced during tensile samples preparation. In different from earlier experiments, here we used a new sample cutting technique to prepare tensile specimens, i.e., nanoseconds pulsed-laser cutting (PLC). The structural characterizations are followed by a full spectrum of tensile property measurements at various strain rates and temperatures. Strength, ductility, strain hardening, and strain rate sensitivity are examined and compared with the recent literature. As the ductility of nc metals is closely tied to their fracture process, which is not well understood at present, we focus particular attention on the fracture patterns of our nc samples. Finally, in-situ synchrotron x-ray diffraction (SXRD) and ultra-small angle x-ray scattering (USAXS) are applied to identify the fundamental deformation mechanisms and void evolutions in these nc metals.[19, 20] The implications of these uncovered experimental results are discussed with the principal purpose of identifying strategies to enhancing the tensile ductility and fracture toughness of nc metals.

II. EXPERIMENTAL DETAILS

The hcp-structured nc cobalt (nominal d~15 nm) and fcc-structured nc nickel (nominal d~20 nm) were acquired from Integran Technologies Inc. (Canada) and Goodfellow Corporation (USA), respectively. Both samples are prepared by a pulsed ED method and have thicknesses on the order of ~150 μm. We have also used nc nickel (nominal d~20 nm) acquired from Integran

Technologies Inc. (Canada) as an independent reference material (herein referred to as ref-nc-nickel). The impurities and the tensile properties of ref-nc-nickel have been reported in ref. [3].[3] The coarse-grained (cg) nickel (99.99+%) was obtained from Goodfellow in as-rolled condition with an initial thickness of ~200 μm, and annealed at 1173 K for 4 hours, leading to an average *d* of 40 μm. The cg cobalt (99.99+%) was also acquired from the same source, and annealed at 1173 K for 4 hours. The average *d* of cg cobalt is 35 μm. To understand the impurity and/or segregation effect on the tensile property of nc cobalt, samples were prepared by annealing nc cobalt at 523 K, 673 K, 773 K, respectively, with a fixed annealing time of 0.5 hour. These annealing temperatures were chosen just below and above the hcp cobalt martensitic phase transformation temperature (i.e., hcp → fcc, 690 K).[21] The annealing experiments were carried out in a vacuum (better than 1×10^{-3} Pa). Similar annealing experiments were performed before for ref-nc-nickel and reported in ref. [3].[3] The composition analysis of both nc metals was performed using inductively coupled plasma mass spectroscopy (ICP-MS) (for metallic impurities) and instrumental gas analysis (IGA) (for light elements H, C, S, N, and O) (Evans Analytical Group, LLC. NY, USA). In IGA analysis, the samples are placed in a ceramic crucible in a high frequency induction furnace where it is heated at a programmable temperature. The combustion of the samples release gases, which are then measured by four infrared (IR) detectors (C and S by combustion-IR, N and H by inert gas fusion-thermal conductivity (IGF-TC), and O by a nondispersive infrared sensor (IGF-NDIR)), after dust and moisture removal.

The tensile tests were carried out on an Instron desktop 4444 screw-driven desktop machine (Norwood, MA, USA) equipped with a 120 N load cell. The deformation strain rate is in the range of 1.0×10^{-7} – 1.0×10^{-1} s^{-1}, spanning six orders of magnitude. Two test temperatures were selected (i.e., room temperature (RT) and 77 K). In order to correct the machine stiffness, the displacement of selected samples was measured with an EIR LE-01 (Electronic Instrument Research, Irwin, PA) Laser extensometer with a 0.1 μm resolution. Two silver-color stripe tapes were placed on the sample surface in order to reflect the laser signal from the extensometer and record the gauge length/displacement. Since the tensile properties of nc and ultrafine-grained (ufg, 1000 nm < *d* <100 nm) materials are closely tied to their sample geometry,[4] the dogbone dimension for all nc specimens is fixed at 5.0 mm long (L) × 2.0 mm wide (W) × 0.12 mm thick (T). Assuming an average *d* of 20 nm, the gauge volume of the tensile sample contains approximately 2.9×10^{14} grains. The tensile samples were cut using two different techniques; i.e.,

wire EDM and PLC. The Lumomics® excimer laser (248 nm wavelength) has a pulse length of 18 ns with 200-250 mJ power. After cutting, the surface of all samples was polished with silicon carbide papers of 400, 600, 800, 1200 metallurgical grits and alumina suspension of 0.5 and 0.1 μm, whereas the sample edges were left in as-cut conditions. The sample gauge surfaces were examined by scanning electron microscopy (SEM) (FEI Nova 600, Oregon, USA) and atomic force microscopy (AFM) (Molecular Imaging, Agilent Tech., USA). In addition to conventional tensile tests, we have also performed in-situ high-energy (E = 80.8715 keV, 0.153589 Å wavelength) SXRD experiments at Sector 1 of the Advanced Photon Source (APS) of Argonne National Laboratory (Argonne, IL, USA). Both nc cobalt and nc nickel samples were loaded in uniaxial tension in a MTS 858 load frame at strain rates ranging from ~ 4×10^{-6} – 3×10^{-4} s^{-1}. The experiments were performed in transmission geometry with an amorphous Si area detector positioned 1103 mm from the nc nickel and 970 mm from the nc cobalt samples. The detector, which is 41 × 41 cm^2 in area, has a 200 × 200 μm^2 pixel size. For all the strain rates, the diffracted intensities were collected in real time during tensile straining. Fig. 1 shows the schematic of the in-situ SXRD setup. Note that the recorded patterns in SXRD experiments correspond to scattering from crystal planes that are approximately normal to the deposition surface, and therefore, are a measure of the in-plane lattice strains during deformation.

To investigate the strain hardening behavior of nc cobalt in compression, RT rolling was carried out on a standard motor roller (Standard Machy Co., Providence, RI) with two position adjustment wheels. The absolute rolling strain is defined as $\varepsilon = \frac{t_0 - t}{t_0} \times 100\%$, where t_0 and t are sample thickness before and after rolling, respectively. The true strain of the rolling can be calculated as $\varepsilon = ln\left(\frac{t}{t_0}\right)$. The Vickers hardness ($H_v$) measurement was performed manually on a LECO LM-100 hardness tester. For each indentation, the pyramid-shaped images were recorded by a ConfiDent Hardness Testing Program and converted to a hardness value. The final reported hardness of each sample is averaged from at least ten measurements.

The out-of-plane texture of both deposits was characterized by means of x-ray diffraction (XRD) (θ – 2θ scan) using a Philips APD3720 Goniometer with Cu K_α radiation. The out-of-plane texture was evaluated through {111}/{200} intensity ratio for nc nickel and {101}/{002} intensity ratio for nc cobalt, after normalized with standard powder diffraction intensities of nickel and cobalt (i.e., 100% random samples), respectively. The microstructure imaging was

performed using a Philips CM-300 FEG transmission electron microscope (TEM) operated at 300 keV. The plan-view TEM samples of nc nickel were prepared by double-jet electropolishing with an electrolytic bath of 25% nitric acid and 75% methanol at a temperature between 233 – 243 K. For nc cobalt, the electrolyte is 23% perchloric acid and 77% acetic acid with the temperature of the solution maintained below 258 K during the electropolishing. The cross-sectional TEM samples of both nc metals were prepared using focused ion beam (FIB) method (FEI Nova 600 Dual-Beam FIB, Oregon, USA). Note that electropolishing or FIB could inevitably introduce nanovoids into specimens during the thinning process. Therefore, these two techniques are not suitable to prepare samples without nanovoid artifacts. Here, we use the USAXS method (a technique sensitive to electron density contrast) to characterize the nanovoid concentration and size distribution in as-deposited and tensile-deformed samples.[22] The USAXS experiments were carried out at Sector 15 of APS (Chicago, IL, USA), with the beam energy of 18 keV (0.69 Å wavelength). The scattering vector q is given by $(4\pi/\lambda)\sin\theta$, where λ is the synchrotron wavelength and 2θ the scattering angle. The end station consists of a Bonse-Hart camera, which can measure q from about 10^{-4}-10^{0} $Å^{-1}$. Data were processed using the codes developed for this USAXS instrument, and included absolute scattering intensity calibration and slit desmearing. The maximum entropy method, implemented in the "Irena" package for SAS data analysis, was used to determine scatter size distributions.[23] The inhomogeneous structure feature size that can be resolved by this technique is approximately 2 nm – 2 μm. For tensile-tested samples, USAXS data were collected near the sample necking areas with the incident beam parallel to the film normal direction. With this measurement configuration, note that elongated voids (if existent at all) along the grain columnar direction are not resolved.

III. RESULTS

A. Impurity, initial microstructure, and tensile sample surface conditions

Literature work has indicated that the tensile property of ED nc metals strongly depends on their processing conditions and impurities,[2, 3] which can be solution-related or even batch-dependent. We have examined the impurity levels of our starting materials, which are complied in Table 2. In addition to metallic impurities (coming from anode or chemicals for electrolytic bath), we have also measured the common light element contaminations such as H, C, N, O and S in both materials. The nc cobalt contains substantially less metallic elements compared to nc Ni, for which the contaminants are strongly batch-dependent. In general, all three types of

samples contain a substantial amount of sulfur, which is a known embrittlement element in ED-synthesized materials. In addition, the nc nickel also has an appreciable amount of hydrogen. Although the direct impact of these impurities on tensile property is poorly understood, the existence of impurities (and/or nanovoids) is expected to impact the electrical conductivity of nc metals, which has a non-negligible effect on tensile sample EDM cutting (as discussed below).

The statistical average *d* from plan-view TEM images of nc cobalt and nc nickel reveals values of 20 ± 9 nm and 28 ± 5 nm, respectively. To envision a complete picture of microstructure, Fig. 2 shows representative cross-sectional TEM images of nc cobalt and nc nickel. For nc cobalt (Fig. 2(a)), the grains are highly equiaxial with very few elongated ones (marked with white arrows). Growth twins are visible inside some grains (one of which is highlighted with a white square). The corresponding selected area electron diffraction (SAED) pattern shown in the inset exhibits generally continuous rings with intensity variations (the aperture diameter is 2.0 μm), consistent with highly equiaxial grains. The grains for nc nickel (Fig. 2(b)) along the cross-section are more or less elongated, with some grains having 1:2 ~ 1:3 aspect ratio. The inset SAED pattern at the lower-left corner shows relatively continuous rings when 2.0 μm diameter selected area aperture is used; but arcs become pronounced when a smaller aperture size (0.4 μm) is chosen (the inset at the lower-right corner). Growth twins are not very common in nc nickel, in contrast with that of nc cobalt. As summarized in Table 3, nc cobalt exhibits a {002} out-of-plane texture with 24% randomness; nc nickel has a {200} out-of-plane texture with 42% randomness. The grain sizes of nc cobalt and nc nickel from cross-sections are 22 ± 10 nm and 47 ± 13 nm, respectively.

The surface roughness, especially the gauge conditions of tensile samples, is critical to the tensile behavior. We have examined the effects of two cutting techniques on gauge edge and surface morphologies of nc cobalt and nc nickel. As demonstrated in Fig. 3, EDM-cutting leads to substantially surface roughening along the gauge edges for both materials, and more importantly, causes pitting with sizes of 10-25 μm on the sample surfaces (see Fig. 3(a) and (d)). Compared to nc nickel, nc cobalt shows a much larger concentration of pits/voids (see inset of Fig. 3(a)), likely due to different electrical conductivity of these two nc materials. Note that EDM-cutting technique strongly depends on the nc materials conductivity, which is sensitive to impurities, voids, and excessive GBs. These results indicate that the defects/voids induced during EDM cutting are materials-dependent; this underscores the importance of exploring tensile

behavior using samples prepared by other cutting techniques. In comparison, no pitting was observed in PLC samples, which show "valley and hill" type of gauge edges with the height variation on the scale of 10 μm (Fig. 3(b)). Within the valleys, however, the surface is nanometer-scale smooth (± 2.5 nm), as determined by AFM. To investigate possible thermal-induced grain growth for both cutting methods, we use FIB ion channeling technique with a very low current ion beam (30 KeV, 9.7 pA).[24] Figs. 3(c), 3(f), and 3(g) indicate that a gradient grain-coarsening layer was formed for PLC samples, the thicknesses of which are ~15 μm for nc cobalt and ~30 μm for nc nickel, respectively, i.e., grain-coarsening is much faster and worse in nc nickel. The largest grain sizes observable for nc cobalt and nc nickel are 2.0 μm and 5.0 μm, respectively. In contrast, no clear grain coarsening is observed for EDM-cut samples except for the very edge, Fig. 3(e). However, pitting/voids due to cutting visibly penetrates through the whole sample. These voids are rather large, and thus could adversely affect the tensile property measurements. From these results, it occurs to us that EDM cutting is more likely to cause internal destructions to nc metals due to their relatively poor conductivity,[25] whereas the PLC limits harms to the sample edges. Our effort to remove grain-coarsening layers in PLC samples using electropolishing caused some pitting and nonuniform thinning of edges. Therefore, these edges were left in as-cut conditions. For rigidity, the tensile test measurements reported here are from the samples cut by PLC method (unless otherwise stated). The strength values are corrected by the observed grain growth data, using a composite model, i.e., $\sigma = V_{nano}\times\sigma_{nano}+V_{coarsened}\times\sigma_{coarsened}$, where V_{nano} and $V_{coarsened}$ are the volume fractions of original nano-grains and coarsened grains, respectively; σ_{nano} and $\sigma_{coarsened}$ are their corresponding flow stresses (assuming the ratio of these two flow stresses is inversely proportional to $\sqrt{d}$). It is estimated from the grain growth investigations that the measured strength values will be reduced by 3.0% for nc nickel, and 1.4% for nc cobalt. Grain coarsening layers could also have impact on the strain hardening behavior of nc materials.[26] To this end, we have prepared tensile samples by manually grinding off the edges with 1200 metallurgical grit sand papers. Comparison experiments revealed negligible differences between as-cut and polished-samples, likely due to the too small volume percentage of coarse grains.

B. Tensile characteristics

The tensile engineering stress-strain curves of nc cobalt, tested at different strain rates and temperatures, are displayed in Fig. 4(a). These curves are from the original tests without correction of the grain growth. Overall, 14 tensile tests were performed in the strain rate range described above (i.e., two tests for each strain rate). For clarity of presentation and to better reveal the tensile-ductility trend, here we select three representative strain rates that cover six orders of magnitude. There are several notable features on these curves: (1) nc cobalt is visibly ductile at all test conditions (including at liquid nitrogen temperature), with ε_{tef} ranging from 0.06-0.11. The quantitative information of the uniform tensile elongation (ε_{unif}) and ε_{tef} is included in Table 3; (2) a strong strain hardening behavior is discerned in all plots, the degree of which is dependent on test parameters; (3) low temperature (i.e., 77 K) or slow strain rate apparently leads to a smaller ε_{tef}, i.e., ε_{tef} increases with increasing strain rate and temperature (see Table 3). This trend disagrees with the literature data,[9] which suggest a decreased ε_{tef} trend with increasing strain rate in the narrow range of 1×10^{-4} – 2.5×10^{-3} s^{-1}. Note that the tensile results reported in ref. [9][9] used samples cut by EDM. In contrast, our test results in the strain rate range of 1×10^{-4} –1×10^{-1} s^{-1} show little difference in terms of ε_{tef} values; (4) with the exception of the sample tested at the highest strain rate (i.e., 1×10^{-1} s^{-1}), nc cobalt exhibits little post-necking elongation (see Table 3), suggesting that it is susceptible to fracture process after the maximum load.

The tensile behavior of nc Ni, also tested under different external conditions and shown in Fig. 4(b), surprisingly duplicates most traits (i.e., (1)-(4) above) recorded in nc cobalt with the following important discrepancies: (1) the overall ε_{tef} (0.02-0.04) of nc nickel is noticeably smaller than those of nc cobalt, so are the 0.2% yield strength ($\sigma_{0.2\%}$) and the ultimate tensile strength (σ_{uts}); (2) our quantitative calculations suggest that the strain hardening and strain rate hardening behavior of these two materials are perceivably different (see Table 3); (3) the ε_{tef} in nc nickel shows little rate-dependent behavior when tested in the strain rate range of 1×10^{-4} – 1×10^{-1} s^{-1}; but seems smaller when tested at the extremely slow strain rate (1×10^{-7} s^{-1}) and low temperature (77 K). This observation supports the GB affected zone model and some prior experiments;[7] but contradictory findings have been reported.[2, 6] Table 3 gathers all the tensile properties of nc cobalt and nc nickel measured from our experiments, after the corrections of strength values from grain growth.

C. Strain hardening and strain rate sensitivity

Assuming a power-law hardening behavior for both nc metals, where the flow stress $\sigma = \sigma_y + K_s\varepsilon^n$ (i.e., Ludwig equation; σ_y represents the yield stress, K_s is the strength coefficient, and n is the strain hardening exponent), we attempted to derive the n values for nc cobalt and nc nickel by using $\log(\sigma-\sigma_y)$ versus $\log(\varepsilon)$ plots. However, we found that in most cases, a good fit was unable to be obtained. For example, for nc nickel tested at 1×10^{-4} s^{-1} and RT, we calculated an n value of 0.23 at the initial 0.01-0.02 strain (below refers to n_1); but decreases down to 0.11 at 0.025-0.035 strain (below refers to n_2). In contrast, a good power-law fit can be obtained for cg nickel. For this reason, the numbers reported in Table 3 are the ranges of values we calculated, using the first 0.01 plastic strain for n_1 (for both nc metals), the 0.02-0.03 plastic strain for n_2 of nc nickel, and the 0.05-0.06 strain for n_2 of nc cobalt. The data of cg cobalt and cg nickel were also measured from our own experiments. For nc cobalt, n falls in the range of 0.14-0.38 at RT. In contrast, we measured an n value of 0.29 for a 99.99% purity cg cobalt, suggesting that n reduces only slightly in the nc regime. Interestingly, we obtained another n value of 0.36 for a cg cobalt after annealing the nc cobalt samples at 1173 K for 4 hours. This n value, however, is not included in Table 3 as the material contains a mixture of fcc and hcp structures and may also have severe contamination-segregation issues (see Section **E**). In comparison, the n value of nc nickel at RT (0.11-0.23), which is 30-50% the value of cg nickel, are appreciably smaller than those of nc cobalt. Low temperature deformation increases the initial n_1 values in both materials, suggestive of a stronger strain hardening behavior.

The strain rate sensitivity of nc cobalt and nc nickel, defined as $m = \left(\frac{\partial log\sigma}{\partial log\dot{\varepsilon}}\right)_{\varepsilon,T}$ (where σ is the flow stress, $\dot{\varepsilon}$ is the strain rate, and T is the temperature), can be calculated from the yield stress at different strain rates and shown in Fig. 5. At RT, the *m* values are 0.024 and 0.018 for nc cobalt and nc nickel, respectively. In ref. [9],[9] a negative *m* was inferred for a smaller grain size nc cobalt (~12 nm). We have therefore carried out independent stress-relaxation experiments to verify the *m* value and measure the activation volume (defined as $V = \frac{\sqrt{3}kT}{m\sigma}$, where k is the Boltzmann constant) of our nc cobalt.[27] At RT, *m* and *V* were found to be 0.025 and $12b^3$ (*b* is the Burgers vector of hcp cobalt), respectively. The *m* value of nc cobalt measured from two independent methods is self-consistent, and numerically larger than that of nc nickel (0.018). When compared to their respective cg values, however, the *m* for nc cobalt shows an appreciable

decrease, whereas nearly four-fold enhancement is observed for nc nickel. The different *m* trends in fcc and hcp nc materials are intriguing and will be discussed more in the later section.

D. Fracture behavior

Because of the flaw-prone nature of nc materials and its relevance to ε_{tef}, it is of critical significance to investigate their fracture behavior at different test conditions. We observe that the dominant failure direction of tensile samples is normal to the tensile axis in both nc metals. Occasionally, fracture oriented 50^0-60^0 towards the tensile axis (e.g., nc nickel tested at 1×10^{-1} s^{-1}) is seen, but is not a common failure mode. Fig. 6 shows the fracture surface of nc cobalt and nc nickel tested at RT and 77 K, respectively. Like many other nc metals, ductile dimples are observed for both nc materials. The size of dimples for nc cobalt is 0.1-0.3 μm at RT, and decreases down to 0.05-0.18 μm at 77 K. In comparison, the dimple sizes for nc nickel are 0.5-1.5 μm at RT, and 0.3-0.8 μm at 77 K, respectively, i.e., they are substantially larger vis-à-vis those of nc cobalt. If we normalize the dimple sizes at RT with the respective plan-view average grain size in both materials, the dimple size in nc cobalt is 3-9 times that of the grain size, whereas this factor is 18-50 times for nc nickel. The low temperature deformation decreases the dimple size by approximate half in both nc materials.

In cg materials, it is known that the tensile deformation of hcp cobalt is mostly controlled by deformation twins, the fracture surface of which can be seen in Fig. 6(c). Slip patterns are difficult to identify, and furthermore, the fracture surface of cg cobalt is topologically rough. In contrast, the plastic deformation of fcc-structured cg nickel is dictated by dislocation slips, where the slip mark is one of the major signatures on the fracture surface (Fig. 6(f)). It is thus interesting to note that dimples are the only failure patterns in both nc metals (with clear size disparity).

E. Annealing effect

Recent literature suggests that elevated temperature annealing can have substantial impact on the tensile properties of ED nc materials.[3, 28, 29] This has been demonstrated in nc nickel but not in nc cobalt. Fig. 7 shows the tensile engineering stress-strain curves of nc cobalt annealed at three different elevated temperatures. Reminiscent of the tensile behavior of nc nickel after annealing,[3] several regimes of tensile behavior in nc cobalt can be identified. The intermediate temperature annealing (523 – 673 K), i.e., below the martensitic transformation temperature of hcp cobalt, notably enhances the tensile strength with slight sacrifice of their

tensile ductility, suggesting that impurity segregation has not severely marred the tensile property. Thermal annealing at higher temperatures (≥ 773 K), however, leads to a drastic drop of both the strength and ductility. This remarkable change of the tensile behavior seems to coincide with the phase-transformation temperature, concurring with grain growth and impurity segregation. Compared to nc nickel,[3] we observe that the impurity segregation in nc cobalt occurs at much higher temperatures. This is understandable, considering that the impurity contents and levels are very different in these two nc metals. The annealing results reported here agree with different grain coarsening behavior uncovered in tensile sample preparation experiments, i.e., nc nickel is much less stable.

F. In-situ SXRD and USAXS measurements

From the tensile results above, we notice that both nc metals show appreciable but different strain hardening and strain rate hardening behavior. We applied in-situ SXRD technique to study the respective deformation mechanisms. Both samples were loaded-unloaded for multiple cycles at two different strain rates (~4×10^{-6} s^{-1} and ~3×10^{-4} s^{-1}). Assuming a Gaussian distribution of inhomogeneous strain,[30] the root-mean-squared (RMS) strain during each individual cycle was calculated based on peak broadening analysis. The texture evolution was quantified according to the peak intensity.[31, 32] The convoluted nature of the diffraction peaks in nc cobalt prevented us from calculating accurate RMS strains. For nc nickel, as shown in Fig. 8, we observe that the initial RMS strain is ~0.31%, and shows a slightly downward trend following each unloading cycle (dashed guide line in the figure). In the last few unloading cycles we examined, the RMS strain becomes ~0.29% (i.e., reduced by ~6%). Note that the samples were broken in the final few cycles. Due to the lack of dislocation accumulations in the grain interior, the RMS strain is likely to arise from elastic variations of the lattice parameter in the grain interiors due to the surrounding GB network.[30] The reduction of RMS strain after multiple cycles suggests a "mechanical annealing" mechanism similar to those observed in microcompression of metallic nanopillars.[33] Due to the subtle change of RMS strains, we did not perceive a clear strain-rate-dependent behavior (i.e., compare Fig. 8(a) to 8(b)).

In addition to RMS strain, we have also examined the residual lattice strain (defined as $\Delta\varepsilon = \varepsilon^{hkl} - \varepsilon_0^{hkl}$, where $\varepsilon^{hkl} = \frac{d^{hkl}-d_0^{hkl}}{d_0^{hkl}}$ is the lattice strain after each unloading cycle, and ε_0^{hkl} is the reference lattice strain before loading) of each plane family normal to the longitudinal direction, which offers a measure of the lattice strain parallel to the tensile axis (see Fig. 1). For

nc nickel in tension, it has been archived that the lattice strain of (111) plane shows a tensile shift, whereas other planes such as (200), (220), and (311) show a compressive shift. In fcc nc materials, (200) is the most compliant plane which has the largest absolute value of lattice strain deviation and has been historically emphasized to investigate the deformation behavior.[31] Fig. 9(a) shows the $\Delta\varepsilon$ of (200) plane in nc nickel as a function of the macroscopic plastic strain (i.e., after the subtraction of the strain contribution from the small applied stress necessary to keep the sample in the grips), presented at two different strain rates. We observe that the residual compressive strain in (200) becomes appreciable after ~0.002 macroscopic strain, and accumulates slightly with each additional loading cycle. This behavior has not been previously documented but is consistent with the appreciable strain hardening behavior seen in nc nickel.[34] Compared to (200), the residual lattice strain deviation of (111) is much smaller ($<120\times10^{-6}$). For nc cobalt, the (110) peak shows the largest $\Delta\varepsilon$ (tensile shift), the residual lattice strains of which at two different strain rates are shown in Fig. 9(b). Interestingly, nc cobalt shows much larger residual strains, concurring with strong {101} texture development along the tensile axis.[31] Deformation twinning, which shows a strong grain size dependent behavior, was identified by high-resolution TEM as the primary deformation mechanism in nc cobalt.[31]

In powder-consolidated nc materials, it is known that the plastic deformation is strongly affected by the void content.[12, 35] However, little is known about the influence of voids in ED materials. Fig. 10 shows the USAXS measurement results obtained for five different nickel samples, four of which were tensile-tested. In Fig. 10(a), the scattering intensity arising from the inhomogeneities in electron density is plotted as a function of the scattering vector q, which shows slightly different background intensity (lower-right corner portions of the curves) due to the thickness variations of the samples. Previous small-angle neutron scattering experiments (a scattering technique sensitive to nuclear scattering length contrast) suggest that, compared to voids, the GBs scattering contribution in powder-consolidated nc metals is relatively small and can generally be ignored.[19, 35] In the case of ED nc metals, high-resolution TEM[36] in the literature has suggested that their GB structure is not different from that of cg materials (i.e., no grain boundary phase exists). In addition, the possible segregation of hydrogen to GBs in ED deposits has little impact on the USAXS scattering intensity. Therefore, the scattering features in the figure can be assumed to be mainly caused by voids instead of GBs. In the low q range of 10^{-4}-10^{-3} $Å^{-1}$, two samples tested at elevated temperatures exhibit reduced scattering intensity,

suggesting that a few micrometer-sized voids might have been formed. In the q range of 0.01-0.06 $Å^{-1}$, we observe clear Guinier scattering, indicative of the voids on the order of ten nanometers. Assuming a spherical void shape and using a maximum entropy algorithm,[23] we calculated voids volume distributions as shown in Fig. 10(b). The results indicate that the as-deposited nc nickel has a small concentration of voids with sizes on the order of 25 nm. This size is comparable with the plan-view average *d*, suggesting that nanovoids dominantly reside between grains and/or columns. These results are in contrast with earlier TEM observations that nanovoids exist inside nanograins.[2] Interestingly, tensile deformation of nc nickel at RT and 77 K generates a relatively large fraction of nanovoids with sizes on the order of ~15 nm (in addition to preexisting voids), i.e., smaller than the *d*. The volume fraction of these newly-formed voids generally increases with decreasing temperatures. Note that we have further calculated the void distribution assuming a void aspect ratio of 2:1 (i.e., elongated voids), the smallest void size will shift slightly to ~12 nm but the general trend remains true. In comparison, we observed nanovoids with smaller sizes (15-20 nm, comparable to *d*) but approximately the same concentration in the as-deposited nc cobalt sample. This suggests that the nanovoids content in nc metals is *d*-dependent and likely also batch-dependent.

G. RT rolling

The strong strain hardening behavior of nc cobalt, which is uncommon compared with other nc metals, is further characterized using RT-rolling experiments. Fig. 11 shows the measured hardness as a function of the rolling strain. The inset is the converted true strain versus flow stress plot (assuming flow stress is one third of the hardness). In this experiment, the largest true strain obtained is ~40%. It can be seen that the strong strain hardening in nc cobalt during the rolling process can be maintained up to ~22% true strain and then slightly levels off. But the strain softening region is never observed in nc cobalt. The n of nc cobalt, which was calculated using the initial 20% true strain, is estimated to be 0.30. This number is slightly higher than the values obtained from tensile experiments. The strong strain hardening behavior of nc cobalt without softening is in contrast with the clear strain softening and grain growth behavior previously reported in nc nickel and nickel alloys during the RT rolling.[37, 38]

IV. DISCUSSIONS

A. Strength and strain rate sensitivity

Although the σ_y of nc metals can be described generally by the Hall-petch (HP) scaling law, the quantitative HP slope (K_{hp}) for each metal remains controversial or even undetermined. The σ_y of nc cobalt reported here is slightly higher than others,[9, 31, 39] whereas the σ_{uts} is lower. These discrepancies could be due to different sample cutting methods used (i.e., EDM vs. PLC). It is also noteworthy mentioning that the strength of nc cobalt is rather sensitive to preexisting stacking faults and twins within the nanograins.[40] Therefore, a single average *d* may not always be able to catch the accurate picture of strength information. The lack of strength data for this metal certainly calls for further studies in the HP scaling law of hcp cobalt.

For nc nickel, the empirical HP formula has been under intensive debate due to the large amount of scattered data available for this monolithic metal.[2, 5, 6, 41-47] Earlier work on the yield strength of nc nickel has been most derived from the hardness measurements due to undersized sample dimensions, and the facts that many samples showed nearly brittle behavior and low strength in tension. To discuss the strength of nc nickel, Fig. 12 shows a HP type of graph, assembled from all available data in the literature, as well as our own data here. Note that we use open and solid symbols to represent the strength data obtained from the hardness measurements (i.e., $\sigma_y = H_v/3$) (Hughes,[41] El-Sherik,[42] Knapp,[44] and Schuh[43]) and from the tensile tests (Ebrahimi,[45] Wang,[5] Schwaiger,[7] Dalla Torre,[2] Shen,[6, 46, 47] and this work[3]), respectively. A close inspection of these data reveals that one could obtain two different HP equations for nickel:

$$\sigma_y = 0.23\ \text{GPa} + 13.33\ \text{GPa/nm}^{-1/2} \times d^{-1/2} \qquad (1)$$

and

$$\sigma_y = 0.078\ \text{GPa} + 6.49\ \text{GPa/nm}^{-1/2} \times d^{-1/2} \qquad (2).$$

Eqn. (1) is obtained by least-squares fitting of the hardness data from Knapp[44] plus the cg data ($d \geq 1000$ nm) from Hughes,[41] Schuh,[43] and our work. Eqn. (2) is calculated using all the data (hardness and tensile results) except for those of Knapp[44] and Wang[5] (which seems to show premature failure). Note that ref. [48][48] reports a HP equation of $\sigma_y = 0.27\ \text{GPa} + 6.23\ \text{GPa/nm}^{-1/2} \times d^{-1/2}$ for nickel. It is apparent from these results that K_{hp} of Eqn. (1) is at odds with others. Considering, however, that nickel is an fcc metal with an expectedly small friction stress (σ_0), we argue that Eqn. (2) seems to be the most reasonable HP relationship. Compared with another well-studied fcc metal copper, which has an HP relationship[49, 50] of $\sigma_y = 0.0255\ \text{GPa} + 3.478$

GPa/nm$^{-1/2}$ × $d^{-1/2}$, nickel has higher σ_0 and K_{hp} values, suggesting that it is more effective to elevate the strength levels in nickel through grain refinement. For clarity, Table 4 lists the HP scaling law of some common fcc and hcp metals.

In Fig. 12, it is further noted that the yield strength obtained from tensile tests (i.e., filled symbols) ubiquitously locates underneath the HP fitting curve. To investigate this phenomenon, we evoke the classical Tabor equation that links the materials hardness (H) with σ_y:

$$H = C \times \sigma_y \qquad (3),$$

where C is the constant of proportionality. The value of C depends on the type of indenter shapes (pyramidal, spherical, conical, etc.) and on the materials n.[51] For strain hardening materials, Tabor further deduces a correlation between Vickers hardness, H_v, and σ_{uts} as[52]

$$\frac{H_v}{\sigma_{uts}} = \frac{2.9}{(1-n)}\left(\frac{1-n}{12.5n}\right)^n \qquad (4).$$

Assuming a power law hardening (i.e., $\sigma_{uts} = \sigma_y + k_s\varepsilon^n$, where ε=n at necking), the ratio of H_v/σ_y can be numerically solved. For commonly obtained H_v values (i.e., pyramidal tips), a C of 3.0 is used (i.e., $H_v = 3\sigma_y$), which is a measure of the strength value at an equivalent strain of 0.08-0.10 [51]. For most nc metals, however, such a strain value would implicate a strength close to σ_{uts}. In Fig. 13, we briefly survey the general trends of H_v/σ_y and H_v/σ_{uts} seen so far for nc metals in the literature. Only the results that contain both hardness and tensile measurements for the same nc nickel and nc cobalt are included. Although the available data points are rather limited, it is plain from these results that the H_v/σ_{uts} ratio is often seen at a value of 3, whereas the ratio of H_v/σ_y maintains above 4, i.e., a modified Tabor equation with a C value of 4 or above would be more reasonable for nc metals.[53, 54] This result is consistent with those reported by Brooks *et al.* [55]

Using eqn. (4), Ludwig equation, HP relationship and the materials parameters for nickel shown in Table 5,[56] we have numerically calculated the H_v/σ_y ratio as a function of grain size (10-100 nm, i.e., different σ_y values) and n, which is given by

$$\frac{H_v}{\sigma_y} = \frac{(1-n)}{2.9}\left(\frac{12.5n}{1-n}\right)^n\left(1 + \frac{K_s n^n}{\sigma_y}\right) \qquad (5).$$

As nc nickel has a measured n value of 0.11-0.23, it is observed in Fig. 14 that a conversion factor C of 3 generally holds true for nc nickel. The single largest uncertainty of these calculations is the yield stress values predicted by the HP relationship (i.e., the accuracy of the HP relationship). To test the validity of our computations, we have also carried out similar

calculations for nc copper (whose materials parameters are also shown in Table 5) and a C factor of 4 was found when n=0.1-0.2. These numerical results suggest that a constant of proportionality between 3-4 remains valid for nc metals. The possible discrepancy between experiments and numerical calculations could originate from a number of uncertainties associated with tensile yield strength measurement as this quantity is rather sensitive to surface defects, sample size, texture, and nanovoids as seen in our nc nickel and nc cobalt. In addition to intrinsic processing-related issues, the difficulty with tensile specimen preparation and the lack of better methods to do so have imposed complications on the widespread results. EDM-cutting of nc metals, in particular, could cause serious artifacts and low strength as evidenced from our experiments. It has also been debated that $\sigma_{0.2\%}$ may not be the best quantity to describe the macroscopic yielding behavior of nc metals.[31, 57-60] For hcp nc metals such as cobalt, extra cautions have to be taken as hcp materials often exhibit tension-compression asymmetry that cannot be ignored when utilizing hardness values to extract the tensile yield strength.[61] In addition, the microstructure anisotropy such as columnar grains in nc nickel has impact on the H_v/σ_y ratios as hardness measurement is typically performed normal to the film plane, whereas the tensile σ_y is measured parallel to the plane. A lower C would be expected if both tests were conducted along the same orientation. Taking into account all the factors above and especially the empirical experimental observations, it seems reasonable to adopt the values of 4 and 3 for the H_v/σ_y and H_v/σ_{uts} ratios of nc metals, respectively. On the other hand, it is also apparent that the hardness measurement approach tends to overestimate the K_{hp}, and that an observably high hardness does not automatically warrant a high tensile strength in nc metals.

The enhanced *m* values of fcc nc metals (e.g, nickel and copper) compared to their cg counterparts are well-known in the literature. Several mechanisms have been proposed to rationalize these experimental observations, including a shift from dislocation mechanisms to GB sliding/diffusion mechanism[62] and partial dislocation nucleation from GB ledges or preexisting GB dislocations (i.e., Asaro and Suresh model).[18] The latter correlates the stacking fault energy (γ_s) with the strength, and the ratio of unstable stacking fault energy (γ_{us}) to γ_s with the twinning tendency.[63] While experimental quantification of GB sliding/diffusion is a challenge, the subtle accumulation of lattice strain along the tensile axis in nc nickel suggests a certain degree of grain rotation/sliding mechanism, which also seems consistent with the larger dimple sizes observed in the fracture surfaces. However, this proposed mechanism is difficult to explicate the slightly

reduced *m* and strong texture accumulations seen in nc cobalt.[31] It is believed that when *d* of nc metals becomes less than 30 nm, the GB mechanism is expected to dominate the plastic deformation. It is unclear whether these mechanisms are diffusion- or partial-dislocation-dictated. The GB-related dislocation nucleation models[18, 60] are apparently able to catch twinning behavior and the enhanced strength in nc cobalt after low-temperature annealing, as the model indicates that the required stress for partial dislocation nucleation increases when it nucleates from stress concentrators or GB ledges compared to preexisting GB dislocations (which could have been annealed away during the heat treatment). Surface defect-induced dislocation nucleation mechanisms have also been considered strain-rate-sensitive.[64] This type of plastic mechanism cannot be completely excluded in nc metals as nanovoids could become dislocation nucleation or sink sources. Due to the inadequate experimental data on hcp nc metals,[65-67] the general trend of *m* in this class of materials remains unsolved.[17, 68]

B. Strain hardening, necking, fracture, and tensile ductility

Our earlier high-resolution TEM suggests that the strong strain hardening in nc cobalt is due to deformation twinning,[31] which offers a sustainable strain hardening mechanism in nc metals (as further demonstrated by our RT-rolling experiments). However, the observed initial higher n in fcc nickel is currently not well-understood; but is likely related to the dislocation exhaustion mechanism(s) since (1) strong dislocation accumulation was not observed in tensile-tested samples; and (2) RMS strain decreases with each loading cycle. This type of hardening mechanism is unlikely sustainable. Interestingly, we also observe that most of our tensile tests show little post-necking elongation. This behavior is at odds with the observations in ufg materials where post-necking elongation usually dominates their tensile deformation.[69] It is therefore important to understand this behavior in order to interpret the tensile ductility of truly nc materials.

Following the analysis of McClintock and Argon for thin sheet samples (width/thickness (W/T) >> 1; our samples have W/T = 15),[70] we note that the majority of our samples failed along the direction perpendicular to the tensile axis, i.e., x-axis direction in Fig. 15. The plane-strain constraint (i.e., necking occurs only along the thickness direction), however, requires that

$$d\varepsilon_{xx} = 0,\ d\varepsilon_{zz} = -d\varepsilon_{yy} \quad (6).$$

According to the von Mises criterion and the plastic stress-strain relationship, it can be shown that under this condition,

$$\sigma_{zz} = (2/\sqrt{3})\bar{\sigma} \qquad (7),$$

where $\bar{\sigma}$ is the equivalent stress. This suggests that the axial stress component would be greater than the flow stress in order for the necking of this kind to occur, which is impossible. Through Mohr's circle construction and in order to afford the plane-strain condition (a condition for which the ratios of stresses are given by $\sigma_{3'3'}/\sigma_{2'2'} = 2$), we could find that necking should occur along a line making an angle of 54.7^0 towards the tensile axis, as shown in Fig. 15. Combined with Hart's linear instability analysis, necking occurs in thin sheet samples when

$$2n/\sigma + m - 1 > 0 \qquad (8).$$

Here σ refers to the tensile stress. The apparently contradictory failure direction from our experiments strongly suggests that the fracture process of many tensile samples was flaw-induced rather than controlled by theoretical necking instability. In such situations, the stress intensity factor (assuming mode I crack) given by

$$K_I = \alpha\sigma_{zz}\sqrt{\pi L_c} \qquad (9),$$

where α is a geometrical constant of order of magnitude unity but dependent on crack geometry, and L_c is the size of an initial crack (in the PLC samples, L_c is on the order of 10 μm)[71]. When K_I surpasses the critical stress intensity factor (K_{IC}), the crack starts to grow and penetrate through the thin samples. Eqn. (9) suggests that the size of flaws along the sample edges and the facture toughness of nc metals will have direct impact on the measured fracture stress, and thus, ε_{tef} values. Furthermore, as pointed out above, EDM cutting could introduce large voids into nc metals that inevitably affect their fracture toughness. These may be some of the primary reasons for the inconsistent ε_{tef} data and different trends reported in the literature even in a widely studied model nc materials such as nickel or copper. It is also important to note that, in PLC samples, the thin grain-coarsened layers (<1 Vol.%) may contribute insignificantly to the strain hardening behavior of nc samples; but could play an important role in reducing the fracture toughness, leading to reduced ε_{tef}. For ufg materials, the samples of which are most often prepared by severe plastic deformation technique[72] and have dimensions of millimeters in thickness (i.e., comparable with the gauge width), the thin-sheet necking instability is no longer reinforced and therefore artificial flaws introduced during the sample preparation could become less relevant.

Nonetheless, size-dependent tensile behavior is frequently observed in nc or ufg materials;[2, 4, 73] one key reason for which could be due to the different W/T ratios used in these samples.

From in-situ TEM observations or MD simulations, models in the literature suggest that dimples and fracture process of nc metals are pertained to the collective shear of certain planes around clustered grains and the extent of nanovoid coalescence (rather than *d*).[36, 74] Smaller dimple sizes would imply smaller average void spacing and/or fewer grains involved in such shearing process. The lack of experimental data on the voids in bulk nc samples has precluded further modeling suggestions on the relevance of the voids sizes and distributions. Our USAXS data have revealed several critical pieces of information that will help us to understand the fracture process in bulk nc metals: (1) the deformation-caused nanovoids are smaller than the average *d*, suggesting that they are located along GBs or triple junctions; (2) higher voids concentration (i.e., smaller average void spacing) is observed in low-temperature deformed nc nickel, qualitatively consistent with smaller dimple sizes observed at 77 K; (3) we did not observe direct correlations between pre-existing nanovoids (perhaps too small volume fraction to be influential) and dimple sizes, as nc nickel and nc cobalt have similar initial voids volume but show clearly different dimple sizes after fracture; (4) it remains unclear at present how different slip/twinning systems affects voids formation. It is conceivable, however, that smaller *d* samples offer more GBs and triple junctions for voids nucleation, and thus are likely to have smaller dimple sizes. This is consistent with the smaller dimple sizes seen in nc cobalt.

Based on eqn. (8), the enhanced *m* in nc nickel at RT is hypothetically beneficial for delaying necking and improving the ε_{tef} of this material. Theoretical analysis by Hutchinson and Neale[75] suggests that *m* has a strong nonlinear effect in governing the post-necking behavior in cylindrical samples. A small enhancement of *m* (for example, *m*=0.03) could lead to very diffusive necking and a large post-necking elongation (>0.10). This strategy has indeed been implemented in ufg materials to stabilize and enhance the tensile ductility.[69, 76] For thin sheet samples, when the fracture/failure is often dictated by surface or edge flaws, the *m* effect seems rather faint. Furthermore, many nc metals show a reduced *m* in the nc regime (such as nc cobalt reported here and many body-centered cubic (bcc) nc metals).[77, 78]

C. Factors influencing the tensile properties and their implications

From the discussions above and eqn. (8), we could conclude that n, which is related to the intrinsic materials behavior, is one of the primary parameters that determine ε_{unif} of nc metals.

Even with thin sheet geometry, necking should occur after true strain reaches n/2. This seems to be true in nc cobalt which shows clearly larger ε_{unif} due to its higher n. An n value of 0.11-0.23 in nc nickel could also promise at least 0.06-0.11 ε_{unif}; however, the experiments measured substantially lower values. This supports our earlier hypothesis that the failure of nc nickel is controlled by fracture process rather than by geometric instability. In fact, substantially less ε_{unif} (i.e., < n/2) has also been witnessed in many other thin sheet nanostructured materials.[79-82] The little post-necking elongation observed in nc cobalt suggests that sample geometry and flaws remain significant in these samples. The fracture-controlled deformation mode in these materials is consistent with the smaller ε_{tef} seen at 77 K for both nc metals despite their respective larger n values, suggesting that the fracture toughness of fcc nc metals is reduced at low temperatures. To increase the strain hardening ability in nc metals, it has been suggested that by reducing γ_s (e.g., by addition of second or third element),[83] larger n values can be obtained, which, in turn, help to enhance ε_{unif}. This strategy is consistent with the larger n value and ε_{unif} seen in nc cobalt compared to nc nickel.

Within the same material, some recent experimental results[84] suggest that the strength, n, and ultimate ductility can be tied to the testing direction of anisotropic microstructures if, for example, columnar grain structures exist (such as in nc nickel). A lower strength but higher compressive ductility was reported when the testing direction is nearly parallel ($<10^o$) to the columnar direction of elongated grains. It is fathomable that the tensile behavior would be different provided that the tensile axis is normal to the film plane. Well-designed and delicate experiments are clearly needed in the future in order to address this issue due to the typical thin film geometry for most nanocrystalline as-deposits.

Artifacts and surface flaws, which are commonly associated with synthesis and specimen-preparations, are known to impact the tensile properties of nc materials. For ED-prepared specimens, this effect was previously considered subtle or negligible due to the technique propensity to fabricate fully-dense materials. Our findings, however, point to three important factors that could impact the tensile results: (1) sample geometry. The plane-strain limitation during the necking of thin sheet samples requires modification of the Hart's criterion (i.e., eqn. (8)) and proves that geometric instability can be the determining factor when the W/T ratios of the tensile samples are large. The critical ratio at which the plane-strain condition is no longer applicable depends on the sizes of plastic zone in front of the cracks (i.e., whether it is

larger or smaller than the sample thickness),[71] which is materials-dependent and requires further investigations; (2) flaws or grain-growth layers at the sample edges that could control the fracture process and the subsequent tensile behavior, even in fully-dense nc materials. As a result, the ductility and the ultimate tensile stress could be directly associated with the flaw sizes and/or *d*. It is therefore not surprising that different ductility trends have been reported in the literature; (3) nanovoids present inside ED nc materials. As shown from our experiments, larger voids can also be introduced through EDM cutting. The influence of these nanovoids on the strain hardening and strain rate sensitivity of the materials remains unclear, and therefore, requires further theoretical and experimental investigations. There is recent evidence in the literature suggesting that nanovoids could completely transform the fracture surface from ductile to brittle patterns.[85] Although this transition was never observed in our nc nickel and nc cobalt, the impacts of these pre-existing or artificially-induced nanovoids on the tensile behavior cannot be ignored. The development of additional nanovoids during the tensile deformation (as revealed by our USAXS data) suggests that there exists considerable strain incompatibility among nanograins during the plastic deformation. This "inherent" problem of nc metals could eventually limit their overall ε_{tef}. To overcome the geometric instability, thicker and higher quality samples are obviously desirable. Indeed, much larger ε_{unif} (0.04-0.06) and ε_{tef} values (0.08-0.11) have been reported in 0.4-2.2 mm thick nc nickel and nickel alloys.[6, 47, 86] These nc materials often exhibit a substantial amount of post-necking elongations, together with large ε_{unif}. These are the encouraging signs that nc metals can have useful tensile ductility if they are scaled up, and the surface flaws can be controlled. Caution remains, though, concerning the structural uniformity of these materials along the cross-section, which was not examined or reported on.

The increased *m* values (sometimes by several folds) that have been seen in fcc (nc nickel and nc copper), hcp (nc zinc), or even in bcc (nc tantalum) metals[87] are valuable assets to help diffuse necking and extend the tensile ductility. With few exceptions,[65, 88] however, the *m* values of nc metals at RT remain too small to be influential. Experimental results for nc nickel indicate[89] that *m* increases nonlinearly with the temperature, which is the primary reason why nc metals exhibit a reduced homologous temperature at which superplastic deformation becomes possible. It would be interesting to investigate how the *m* value influences the ε_{tef} of nc metals at a temperature that is well below the superplastic temperature region in thin sheet samples.

V. CONCLUSIONS

Through carefully documenting the tensile behavior of two different crystallographic nc metals, both of which were cut by PLC instead of EDM method, we found that the plastic deformation of nc metals strongly relies on their crystallographic structure in the ways that are fundamentally different from cg materials. Some key findings of this work can be summarized as follows:

1) Nc metals have intrinsic imperfections in as-synthesized state including nanovoids (comparable to ~*d*), texture, and impurities (both are batch-dependent). In addition, extrinsic surface defects, large voids, and coarsened grains can be induced by sample cutting. All of above artifacts influence tensile yield strength and tensile ductility.

2) Intrinsic factors influencing the tensile ductility of nc metals include: (a) strain hardening exponent (n); (b) thin sheet geometry, which has important implications in determining the necking instability and failure orientation; (c) strain incompatibility between nanograins, leading to voids formation, coalescence, and dimple patterns, which are strongly temperature-dependent; and (d) strain rate sensitivity *(m*) of nc materials, which was found to increase in nc nickel compared to their cg counterparts, whereas a reduced *m* is observed for nc cobalt. Despite clearly reduced tensile ductility in nc monolithic materials, they are intrinsically ductile and expected to have enhanced ε_{tef} if geometric instability and sample-cutting induced flaws can be suppressed.

3) The Tabor relationship is re-visited in nc metals. A conversion factor of 4 was identified from experiments, whereas the numerical simulations based on the Tabor model indicate a value of 3 for nc metals. The apparent inconsistency is reconciled by the experimental uncertainties including flaws, sample geometry, tensile-compression asymmetry, and macroscopic yield criterion applicability. A new H-P scaling law is proposed for nc nickel based on our own findings.

ACKNOWLEDGEMENT

The magnanimous help of the following people are gratefully acknowledged: N. Teslich and D. Ahre for FIB and tensile sample preparations, M.F. Bessser, M.J. Kramer, and J. Almer for in-situ SXRD experiments, and J. Ilavsky for USAXS experiments and fruitful discussions. The project is benefited from one of the co-authors' (Y.M.W.) early discussions with Dr. E. Ma (JHU). This work was performed under the auspices of the U.S. Department of Energy by Lawrence Livermore National Laboratory under Contract DE-AC52-07NA27344. The work at Ames Laboratory was supported by the U.S. Department of Energy, Office of Basic Energy

Science, Division of Materials Sciences and Engineering under Contract No. DE-AC02-07CH11358. The APS was supported by the U.S. Department of Energy under Contract DE-AC02-06CH11357.

References

[1] J. R. Weertman, D. Farkas, K. Hemker, H. Kung, M. Mayo, R. Mitra, and H. Van Swygenhoven, MRS Bull. **24**, 44 (1999).

[2] F. Dalla Torre, H. Van Swygenhoven, and M. Victoria, Acta Mater. **50**, 3957 (2002).

[3] Y. M. Wang, S. Cheng, Q. M. Wei, E. Ma, T. G. Nieh, and A. Hamza, Scr. Mater. **51**, 1023 (2004).

[4] Y. H. Zhao, Y. Z. Guo, Q. Wei, A. M. Dangelewiez, Y. T. Zhu, T. G. Langdon, Y. Z. Zhou, E. J. Lavernia, and C. Xu, Scr. Mater. **59**, 627 (2008).

[5] N. Wang, Z. R. Wang, K. T. Aust, and U. Erb, Mater. Sci. Eng. A **237**, 150 (1997).

[6] X. X. Shen, J. S. Lian, Z. H. Jiang, and Q. Jiang, Mater. Sci. Eng. A **487**, 410 (2008).

[7] R. Schwaiger, B. Moser, M. Dao, N. Chollacoop, and S. Suresh, Acta Mater. **51**, 5159 (2003).

[8] L. Lu, S. X. Li, and K. Lu, Scr. Mater. **45**, 1163 (2001).

[9] A. A. Karimpoor, U. Erb, K. T. Aust, and G. Palumbo, Scr. Mater. **49**, 651 (2003).

[10] F. Sansoz and K. D. Stevenson, Phys. Rev. B **83**, 224101 (2011).

[11] S. Van Petegem, F. Dalla Torre, D. Segers, and H. Van Swygenhoven, Scr. Mater. **48**, 17 (2003).

[12] I. A. Ovid'ko, A. G. Sheinerman, and N. V. Skiba, Acta Mater. **59**, 678 (2010).

[13] L. A. Zepeda-Ruiz, E. Chason, G. H. Gilmer, Y. M. Wang, H. W. Xu, A. Nikroo, and A. V. Hamza, Appl. Phys. Lett. **95**, 151910 (2009).

[14] M. Dao, L. Lu, R. J. Asaro, J. T. M. De Hosson, and E. Ma, Acta Mater. **55**, 4041 (2007).

[15] T. Zhu and J. Li, Prog. Mater Sci. **55**, 710 (2010).

[16] T. J. Rupert, D. S. Gianola, Y. Gan, and K. J. Hemker, Science **326**, 1686 (2009).

[17] G. P. Zheng, Y. M. Wang, and M. Li, Acta Mater. **53**, 3893 (2005).

[18] R. J. Asaro and S. Suresh, Acta Mater. **53**, 3369 (2005).

[19] E. Jorra, H. Franz, J. Peisl, G. Wallner, W. Petry, R. Birringer, H. Gleiter, and T. Haubold, Philos. Mag. B-Phys. Condens. Matter Stat. Mech. Electron. Opt. Magn. Prop. **60**, 159 (1989).

[20] P. G. Sanders, J. A. Eastman, and J. R. Weertman, Acta Mater. **45**, 4019 (1997).

[21] W. Bollmann, Acta Metall. **9**, 972 (1961).

[22] T. M. Willey, D. M. Hoffman, T. van Buuren, L. Lauderbach, R. H. Gee, A. Maiti, G. E. Overturf, L. E. Fried, and J. Ilavsky, Propellants Explos. Pyrotech. **34**, 406 (2009).

[23] J. Ilavsky and P. R. Jemian, J. Appl. Crystallogr. **42**, 347 (2009).

[24] C. J. Shute, B. D. Myers, S. Xie, T. W. Barbee, A. M. Hodge, and J. R. Weertman, Scr. Mater. **60**, 1073 (2009).

[25] L. Lu, Y. F. Shen, X. H. Chen, L. H. Qian, and K. Lu, Science **304**, 422 (2004).

[26] T. H. Fang, W. L. Li, N. R. Tao, and K. Lu, Science **331**, 1587 (2011).

[27] Y. M. Wang and E. Ma, Appl. Phys. Lett. **85**, 2750 (2004).

[28] U. Klement, U. Erb, A. M. ElSherik, and K. T. Aust, Mater. Sci. Eng. A **203**, 177 (1995).

[29] A. J. Detor and C. A. Schuh, Acta Mater. **55**, 4221 (2007).

[30] P. M. Derlet, S. Van Petegem, and H. Van Swygenhoven, Phys. Rev. B **71**, 024114 (2005).

[31] Y. M. Wang, R. T. Ott, A. V. Hamza, M. F. Besser, J. Almer, and M. J. Kramer, Phys. Rev. Lett. **105**, 215502 (2010).

[32] S. Cheng, et al., Phys. Rev. Lett. **103**, 035502 (2009).

[33] Z. W. Shan, R. K. Mishra, S. A. S. Asif, O. L. Warren, and A. M. Minor, Nature Mater. **7**, 115 (2008).

[34] Z. Budrovic, H. Van Swygenhoven, P. M. Derlet, S. Van Petegem, and B. Schmitt, Science **304**, 273 (2004).

[35] P. G. Sanders, J. A. Eastman, and J. R. Weertman, Acta Mater. **46**, 4195 (1998).

[36] K. S. Kumar, S. Suresh, M. F. Chisholm, J. A. Horton, and P. Wang, Acta Mater. **51**, 387 (2003).

[37] L. Li, et al., Acta Mater. **57**, 4988 (2009).

[38] X. L. Wu, Y. T. Zhu, Y. G. Wei, and Q. Wei, Phys. Rev. Lett. **103**, 205504 (2009).

[39] G. J. Fan, L. F. Fu, D. C. Qiao, H. Choo, P. K. Liaw, and N. D. Browning, Scr. Mater. **54**, 2137 (2006).
[40] J. Sort, A. Zhilyaev, M. Zielinska, J. Nogues, S. Surinach, J. Thibault, and M. D. Baro, Acta Mater. **51**, 6385 (2003).
[41] G. D. Hughes, S. D. Smith, C. S. Pande, H. R. Johnson, and R. W. Armstrong, Scr. Metall. **20**, 93 (1986).
[42] A. M. Elsherik, U. Erb, G. Palumbo, and K. T. Aust, Scr. Metall. Mater. **27**, 1185 (1992).
[43] C. A. Schuh, T. G. Nieh, and T. Yamasaki, Scr. Mater. **46**, 735 (2002).
[44] J. A. Knapp and D. M. Follstaedt, J. Mater. Res. **19**, 218 (2004).
[45] F. Ebrahimi, G. R. Bourne, M. S. Kelly, and T. E. Matthews, Nanostruct. Mater. **11**, 343 (1999).
[46] C. D. Gu, J. S. Lian, Z. H. Jiang, and Q. Jiang, Scr. Mater. **54**, 579 (2006).
[47] X. X. Shen, C. D. Gu, J. S. Lian, Q. Jiang, Z. H. Jiang, and L. Y. Qin, J. Appl. Phys. **108**, 054319 (2010).
[48] C. A. Schuh, T. G. Nieh, and H. Iwasaki, Acta Mater. **51**, 431 (2003).
[49] M. A. Meyers and K. K. Chawla, *Mechanical Metallurgy* (Prentice-Hall, Inc., Englewood Cliffs, New Jersey, 1984).
[50] S. Cheng, E. Ma, Y. M. Wang, L. J. Kecskes, K. M. Youssef, C. C. Koch, U. P. Trociewitz, and K. Han, Acta Mater. **53**, 1521 (2005).
[51] A. G. Atkins and D. Tabor, J. Mech. Phys. Solids **13**, 149 (1965).
[52] D. Tabor, J. Inst. Met. **79**, 1 (1951).
[53] T. J. Rupert and C. A. Schuh, Acta Mater. **58**, 4137 (2010).
[54] T. J. Rupert, J. A. Trenkle, and C. A. Schuh, Acta Mater. **59**, 1619 (2011).
[55] I. Brooks, P. Lin, G. Palumbo, G. D. Hibbard, and U. Erb, Mater. Sci. Eng. A **491**, 412 (2008).
[56] C. Moosbrugger, *Atlas of stress-strain curves* (ASM International, Materials Park, OH, 2002).
[57] S. Brandstetter, H. Van Swygenhoven, S. Van Petegem, B. Schmitt, R. Maass, and P. M. Derlet, Adv. Mater. **18**, 1545 (2006).
[58] L. Thilly, S. Van Petegem, P. O. Renault, F. Lecouturier, V. Vidal, B. Schmitt, and H. Van Swygenhoven, Acta Mater. **57**, 3157 (2009).
[59] L. Li, P. M. Anderson, M. G. Lee, E. Bitzek, P. Derlet, and H. Van Swygenhoven, Acta Mater. **57**, 812 (2009).
[60] G. Saada and T. Kruml, Acta Mater. **59**, 2565 (2011).
[61] S. Sandlobes, S. Zaefferer, I. Schestakow, S. Yi, and R. Gonzalez-Martinez, Acta Mater. **59**, 429 (2011).
[62] Y. J. Wei, A. F. Bower, and H. J. Gao, Acta Mater. **56**, 1741 (2008).
[63] H. Van Swygenhoven, P. M. Derlet, and A. G. Froseth, Nature Mater. **3**, 399 (2004).
[64] T. Zhu, J. Li, A. Samanta, A. Leach, and K. Gall, Phys. Rev. Lett. **100**, 025502 (2008).
[65] X. Zhang, H. Wang, R. O. Scattergood, J. Narayan, C. C. Koch, A. V. Sergueeva, and A. K. Mukherjee, Appl. Phys. Lett. **81**, 823 (2002).
[66] D. Jia, Y. M. Wang, K. T. Ramesh, E. Ma, Y. T. Zhu, and R. Z. Valiev, Appl. Phys. Lett. **79**, 611 (2001).
[67] A. V. Sergueeva, V. V. Stolyarov, R. Z. Valiev, and A. K. Mukherjee, Scr. Mater. **45**, 747 (2001).
[68] G. P. Zheng, Acta Mater. **55**, 149 (2007).
[69] Y. M. Wang and E. Ma, Acta Mater. **52**, 1699 (2004).
[70] F. A. McClintock and A. S. Argon, *Mechanical behavior of materials* (Addison-Wesley Publishing Company, Inc., Reading, MA, USA, 1966).
[71] T. H. Courtney, *Mechanical behavior of materials* (McGraw-Hill Companies, Inc., Boston, MA, USA, 2000).
[72] R. Valiev, Nature Mater. **3**, 511 (2004).
[73] H. Q. Li and F. Ebrahimi, Appl. Phys. Lett. **84**, 4307 (2004).
[74] A. Hasnaoui, H. Van Swygenhoven, and P. M. Derlet, Science **300**, 1550 (2003).
[75] J. W. Hutchinson and K. W. Neale, Acta Metall. **25**, 839 (1977).

[76] Y. Champion, C. Langlois, S. Guerin-Mailly, P. Langlois, J. L. Bonnentien, and M. J. Hytch, Science **300**, 310 (2003).
[77] Q. Wei, L. Kecskes, T. Jiao, K. T. Hartwig, K. T. Ramesh, and E. Ma, Acta Mater. **52**, 1859 (2004).
[78] Q. Wei, S. Cheng, K. T. Ramesh, and E. Ma, Mater. Sci. Eng. A **381**, 71 (2004).
[79] A. Misra and R. G. Hoagland, J. Mater. Sci. **42**, 1765 (2007).
[80] A. Misra, X. Zhang, D. Hammon, and R. G. Hoagland, Acta Mater. **53**, 221 (2005).
[81] J. Rajagopalan, J. H. Han, and M. T. A. Saif, Science **315**, 1831 (2007).
[82] N. A. Mara, D. Bhattacharyya, R. G. Hoagland, and A. Misra, Scr. Mater. **58**, 874 (2008).
[83] F. Ebrahimi, Z. Ahmed, and H. Li, Appl. Phys. Lett. **85**, 3749 (2004).
[84] H. Q. Li, et al., Scr. Mater. **65**, 1 (2011).
[85] R. C. Hugo, H. Kung, J. R. Weertman, R. Mitra, J. A. Knapp, and D. M. Follstaedt, Acta Mater. **51**, 1937 (2003).
[86] H. Wei, G. D. Hibbard, G. Palumbo, and U. Erb, Scr. Mater. **57**, 996 (2007).
[87] Q. Wei, Z. L. Pan, X. L. Wu, B. E. Schuster, L. J. Kecskes, and R. Z. Valiev, Acta Mater. **59**, 2423 (2011).
[88] R. Z. Valiev, I. V. Alexandrov, Y. T. Zhu, and T. C. Lowe, J. Mater. Res. **17**, 5 (2002).
[89] Y. M. Wang, A. V. Hamza, and E. Ma, Acta Mater. **54**, 2715 (2006).

Table 1 Selected physical properties of polycrystalline cobalt and nickel[(1)]

	Melting temperature (K)	Young's modulus (GPa)	Shear modulus (GPa)	Bulk modulus (GPa)	Poison's ratio	Density (g/cm^3)	Coefficient of thermal expansion (K^{-1})	Electrical conductivity (S m^{-1})	Percentage of copper conductivity
Cobalt	1768	209	75	180	0.31	8.900	13.0×10^{-6}	1.67×10^{7}	28.7%
Nickel	1728	200	76	180	0.31	8.908	13.4×10^{-6}	1.39×10^{7}	23.9%

(1) These data are adopted from http://www.webelements.com/ (accessed in March, 2011).

Table 2 Impurity levels in nc cobalt and nc nickel, as measured by ICP-MS and IGA methods

Nc cobalt (ppm)		Nc nickel (ppm)		Ref-nc-nickel (ppm)	
H	13	H	34	H	-
C	30	C	91	C	1820
N	<10	N	-	N	<
O	55	O	-	O	50
Na	<10	Na	<10	Al	10
Mg	2	Al	18	S	460
Al	3	Si	<10	Fe	160
Si	<10	P	30	Co	270
P	<10	S	310	Mo	150
S	420	K	<10	W	<
K	<10	Ca	<10		
Ca	<10	Cr	6		
Fe	<10	Mn	3		
Ni	39	Fe	80		
Cu	18	Co	1000		
Zn	77	Cu	72		
As	<100	Zn	210		
Mo	3	As	<10		
Cd	2	Ag	5		
Sn	5	W	84		
Pb	48	Pb	4		

Table 3 Tensile properties of nc cobalt and nc nickel at various strain rates and temperatures. The data of cg cobalt and cg nickel were from our own measurements. The strength values are corrected by considering the grain-growth layers.

Materials	Grain size (nm) (plan-view TEM)	Texture (out-of-plane)	Strain rate (s^{-1})	Temperature	0.2% yield strength ($\sigma_{0.2\%}$, MPa)	Ultimate tensile strength (σ_{uts}, MPa)	Uniform tensile elongation (ε_{unif})	Tensile elongation to failure (ε_{tef})	Strain hardening exponent (n)	Strain rate sensitivity (m)
nc cobalt	20 ± 9	24%	4×10^{-7}	RT	904	1579	0.069	0.069	0.14-0.38	0.025
			1×10^{-4}	RT	967	1720	0.094	0.095		
			1×10^{-3}	RT	1040	1725	0.093	0.093		
			1×10^{-2}	RT	1145	1735	0.079	0.079		
			1×10^{-1}	RT	1228	1795	0.080	0.102		
			1×10^{-4}	77 K	1735	2521	0.058	0.058	0.15-0.49	-
cg cobalt	35×10^{3}	-	1×10^{-4}	RT	274	892	0.26	0.28	0.29	0.034[(1)]
			1×10^{-4}	77 K	388	957	0.14	0.14	0.40	-
nc nickel	28 ± 5	42%	1×10^{-7}	RT	759	1036	0.020	0.021	0.11-0.23	0.018
			1×10^{-4}	RT	866	1316	0.036	0.038		
			1×10^{-3}	RT	898	1357	0.036	0.037		
			1×10^{-2}	RT	930	1393	0.037	0.039		
			1×10^{-1}	RT	978	1406	0.030	0.034		
			1×10^{-4}	77 K	1275	1592	0.022	0.023	0.24	0.003
cg nickel	40×10^{3}	-	1×10^{-4}	RT	58	437	0.30	0.48	0.39	0.005
			1×10^{-4}	77 K[(2)]	70	-	-	-	0.47	0.003

[(1)] This value was measured from our own cg cobalt with 99.99% purity.

[(2)] The test of cg nickel at 77 K was stopped at 23% tensile strain. Hence, the values of σ_{uts}, ε_{unif}, and ε_{tef} were not obtained.

Table 4 A tabulation of HP relationship for some metals from this work and the literature

Materials	Frictional stress (σ_0, GPa)	Hall-petch slope (K_{hp}, GPa/nm$^{-1/2}$)	Reference
Nickel (fcc)	0.078	6.49	this work
Copper (fcc)	0.0255	3.478	[49]
Cobalt (hcp)	0.432	1.90(1)	[31]
Titanium (hcp)	0.0785	12.65	[49]

(1) This value was only derived in the nc regime.

Table 5 Materials parameters of nickel and copper used for Tabor equation calculation

Materials	Frictional stress (σ_0, GPa)	Hall-petch slope (K_{hp}, GPa/nm$^{-1/2}$)	Strength coefficient (K_s, GPa)
Nickel	0.0780	6.490	0.138(1)
Copper	0.0255	3.478	0.530

(1) This value is adopted from ref. [56][56] for a cg nickel with n=0.387.

Figure captions

Fig. 1 The schematic presentation of in-situ SXRD setup. The longitudinal direction in the figure refers to the direction parallel to the tensile axis, which measures the lattice strain of the planes normal to the tensile axis, whereas the transverse direction measures the lattice strain of the planes parallel to the tensile axis.

Fig. 2 Cross-sectional TEM images of (a) nc cobalt, and (b) nc nickel. The corresponding insets are the selected area electron diffraction (SAED) patterns of these two materials acquired with a selected aperture diameter of 2.0 μm (lower-left corner). The inset on the lower-right corner of (b) is the SAED pattern acquired with a 0.4 μm diameter aperture. Note the slightly elongated grains in nc nickel.

Fig. 3 The effects of sample-preparation techniques on the surface conditions, (a)-(d). (a) and (d), SEM micrographs of gauge edges of nc cobalt and nc nickel cut by EDM, respectively. Note the sizable pitting on the surfaces of both samples. The inset in (a) is a lower-magnification image of the side surface of nc cobalt after cutting, showing a high concentration of pitting voids. (b) SEM image of nc cobalt after PLC. No pitting was observed. (c) and (f), FIB ion-channeling images of nc cobalt and nc nickel after PLC, respectively, showing grain growth gradient layers. (g) A higher magnification FIB ion-channeling image of grain growth layer in nc nickel after laser cutting. (e) FIB ion-channeling image of nc nickel after EDM-cutting. No clear grain growth layer was observed. A couple of large grains are accentuated inside the rectangle on the upper-

right corner. Note that all the samples in (a)-(f) are oriented in the same direction (i.e., 60^0-tilted view), with the cutting edge on the top side of the images. In (g), the cutting-edge is located at the left-hand side of the image.

Fig. 4 Tensile engineering stress-strain curves of (a) nc cobalt, and (b) nc nickel tested in the strain rate range of 1×10^{-7} - 1×10^{-1} s^{-1} and two different temperatures (i.e., RT and 77 K).

Fig. 5 A logarithmic plot to estimate the strain rate sensitivity (*m*) of (a) nc cobalt, and (b) nc nickel.

Fig. 6 SEM fracture micrographs of (a) nc cobalt tested at 1×10^{-4} s^{-1} and RT; (b) nc cobalt tested at 1×10^{-4} s^{-1} and 77 K; (c) cg cobalt tested at 1×10^{-4} s^{-1} and RT; (d) nc nickel tested at 1×10^{-4} s^{-1} and RT; (e) nc nickel tested at 1×10^{-4} s^{-1} and 77 K; and (f) cg nickel tested at 1×10^{-4} s^{-1} and RT.

Fig. 7 Tensile engineering stress-strain curves of nc cobalt annealed at different temperatures.

Fig. 8 The root-mean-squared (RMS) strains of nc nickel as a function of loading-unloading cycles at the strain rate of (a) 4×10^{-6} s^{-1}, and (b) 3×10^{-4} s^{-1}, respectively.

Fig. 9 The longitudinal residual lattice strains of (a) (200) planes of nc nickel, and (b) (110) planes of nc cobalt as a function of the macroscopic plastic strain, acquired at two different strain rates.

Fig. 10 USAXS results obtained for five independent nickel samples with (a) the scattering intensity plotted as a function of the scattering factor (q), and (b) the calculated void size distribution using a maximum entropy algorithm. We note from our experiments that the voids size distribution is relatively sensitive to the synchrotron beam location relevant to the necking region and the shape assumption during the modeling. Therefore, the plots in (b) do not offer absolute value comparisons between samples.

Fig. 11 The hardness as a function of rolling strain for nc cobalt at RT. The inset is the converted true flow stress versus true strain in nc cobalt during the rolling process.

Fig. 12 Hall-petch type graphs of monolithic nickel with the data from the literature and our work. Two linear fitting curves were calculated from these data with a respective HP slope of 13.33 GPa/nm$^{-1/2}$ and 6.49 GPa/nm$^{-1/2}$. The solid symbols are data obtained directly from tensile tests, the majority of which are found lying underneath the HP fitting curves as accented inside the ellipse.

Fig. 13 A survey of Vickers hardness (H_v) versus the yield stress (σ_y), and Vickers hardness versus the ultimate tensile stress (σ_{uts}) ratios of nc nickel and nc cobalt.

Fig. 14 The numerical calculation of the Tabor relationship for nc nickel, assuming different strain hardening exponents and different grain sizes. See the text for detailed discussions.

Fig. 15 A schematic of necking geometry and stress analysis in thin sheet samples (W/T>>1).

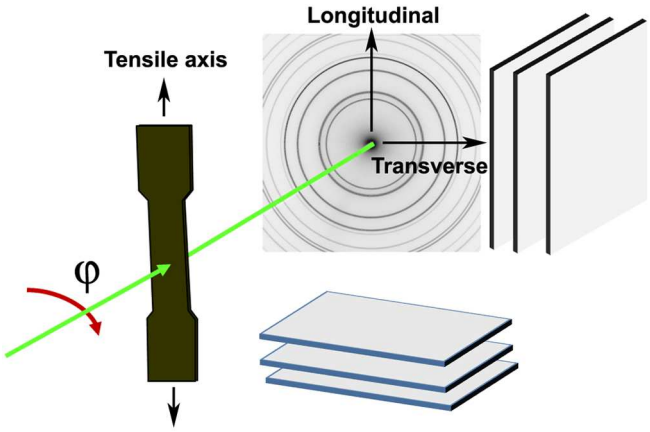

Figure 1 BF11812 30NOV2011

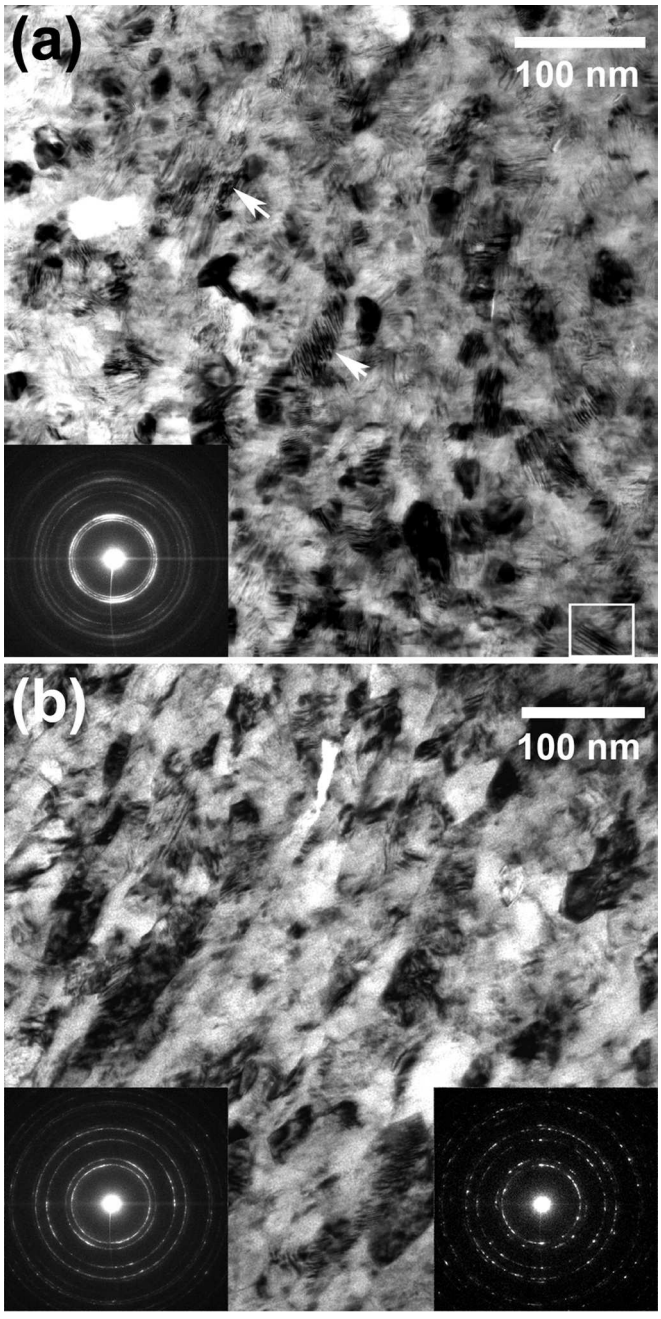

Figure 2 BF11812 30NOV2011

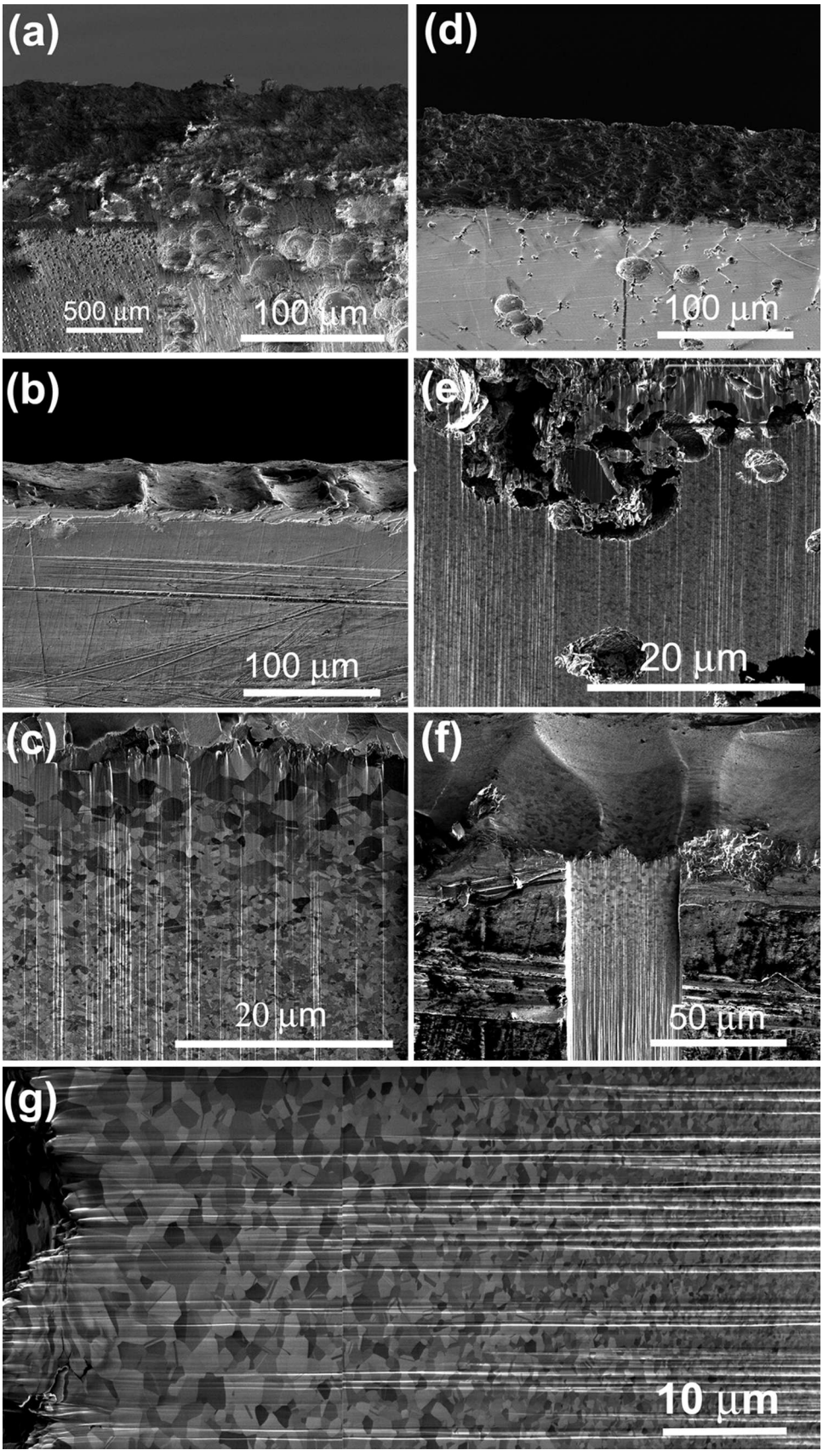

Figure 3 BF11812 30NOV2011

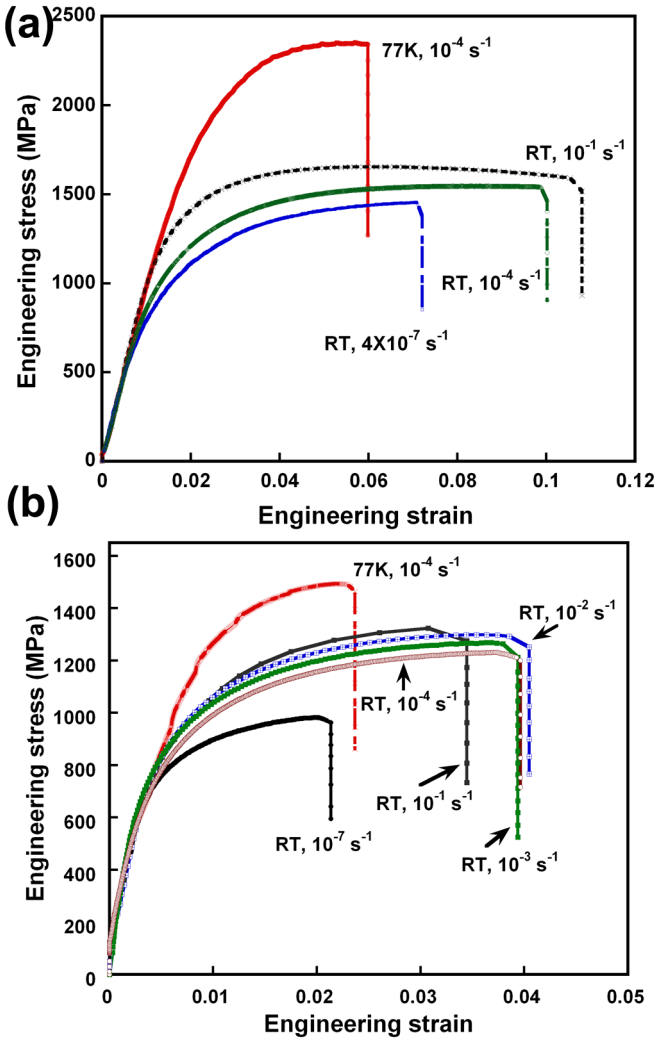

Figure 4 BF11812 30NOV2011

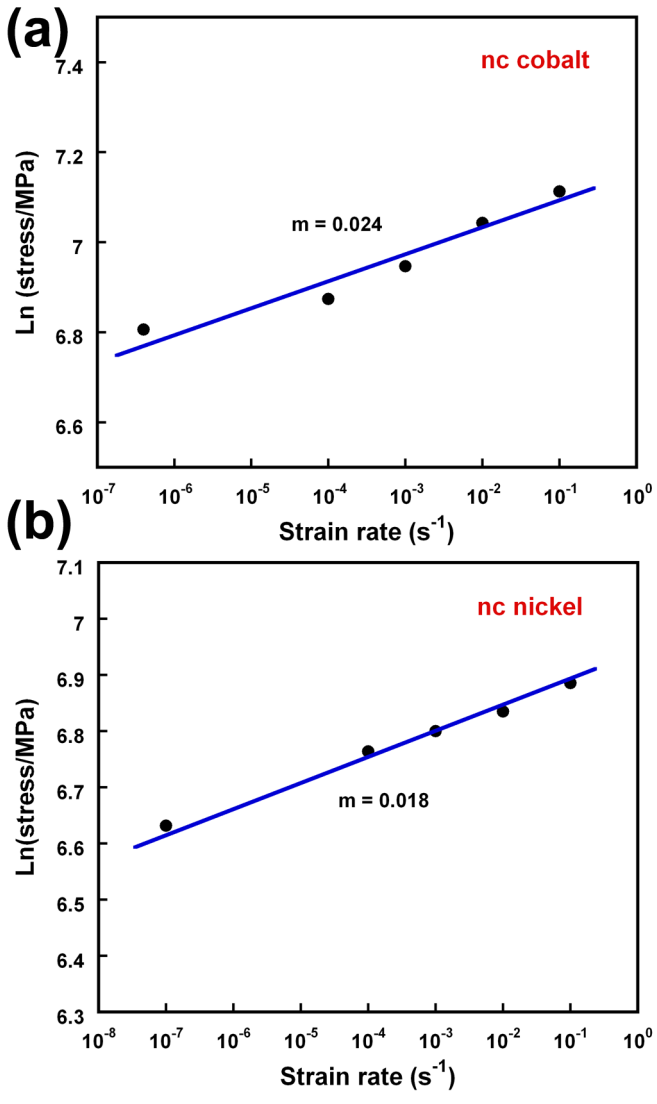

Figure 5 BF11812 30NOV2011

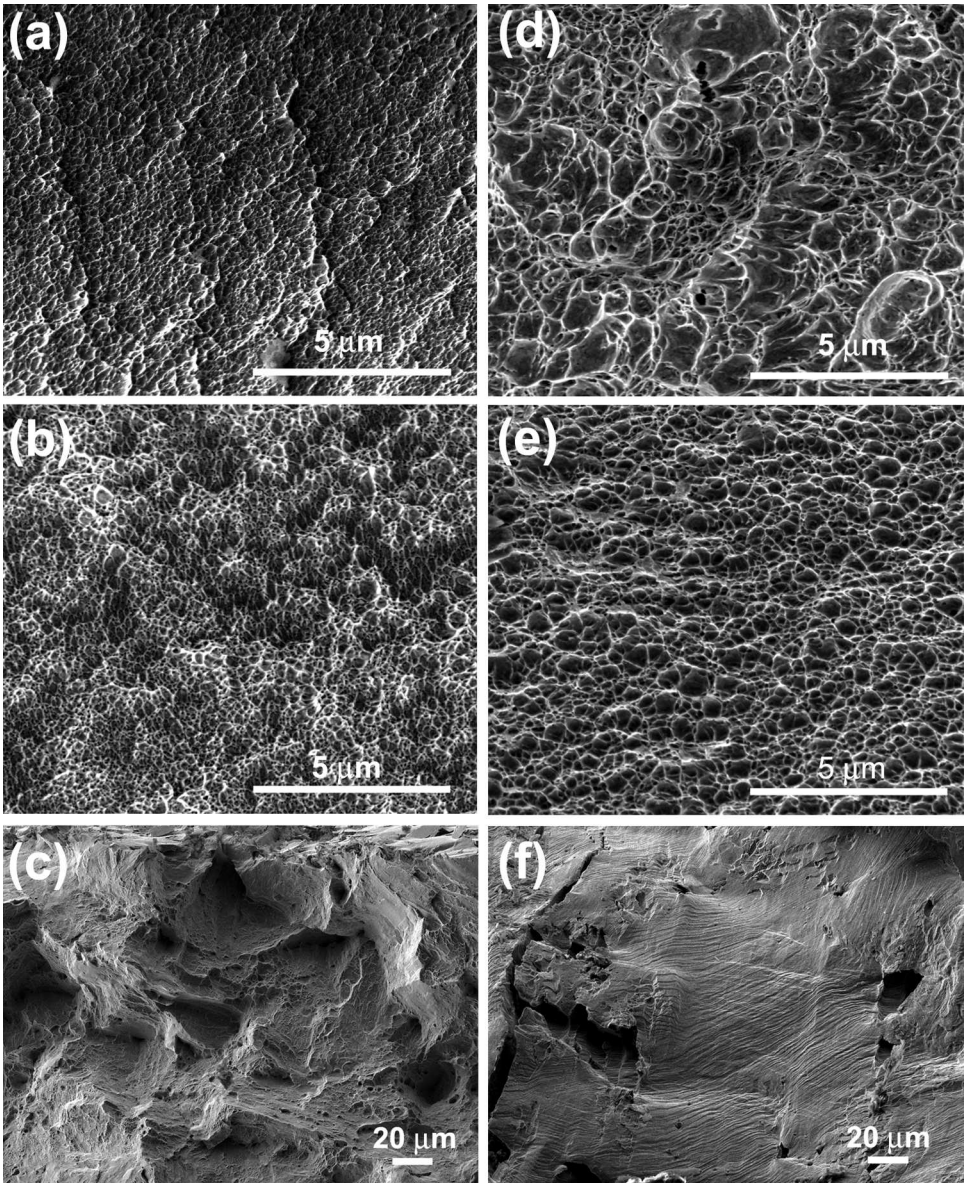

Figure 6 BF11812 30NOV2011

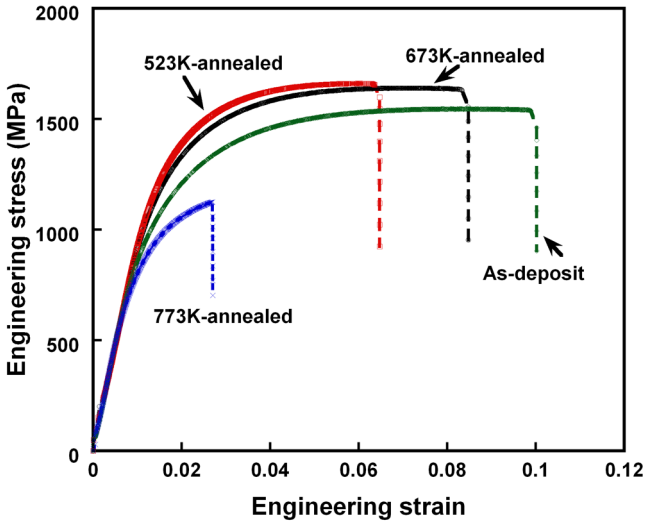

Figure 7 BF11812 30NOV2011

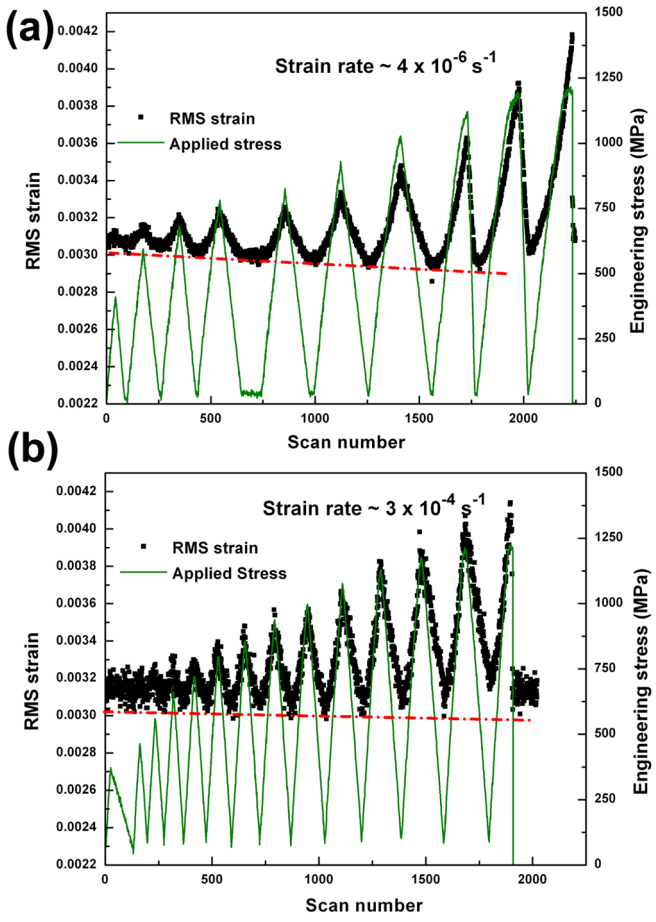

Figure 8 BF11812 30NOV2011

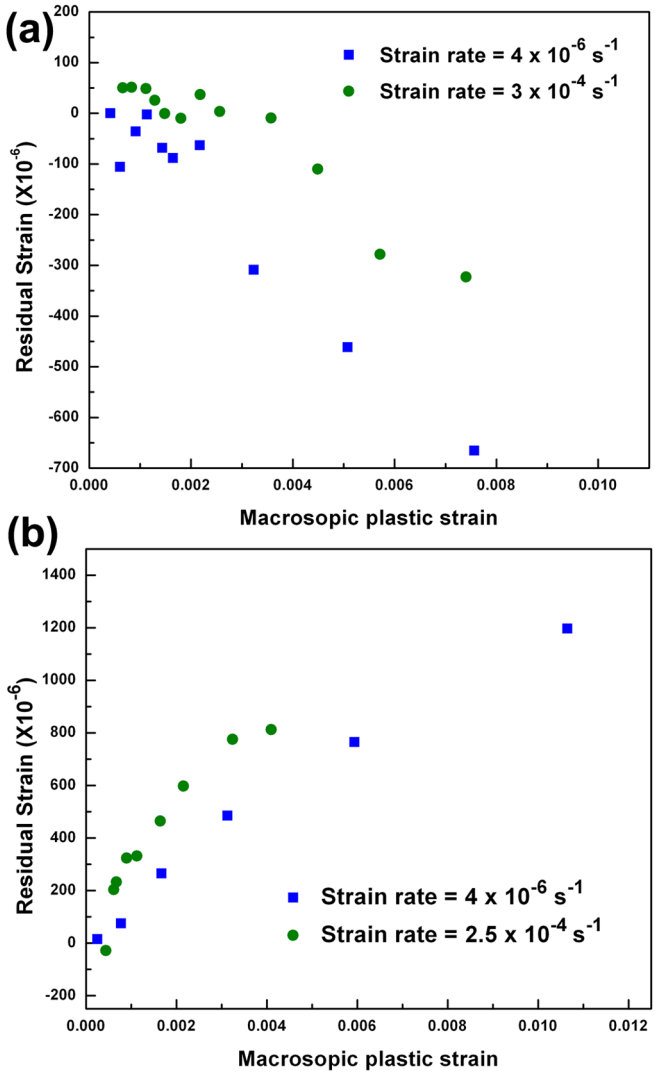

Figure 9 BF11812 30NOV2011

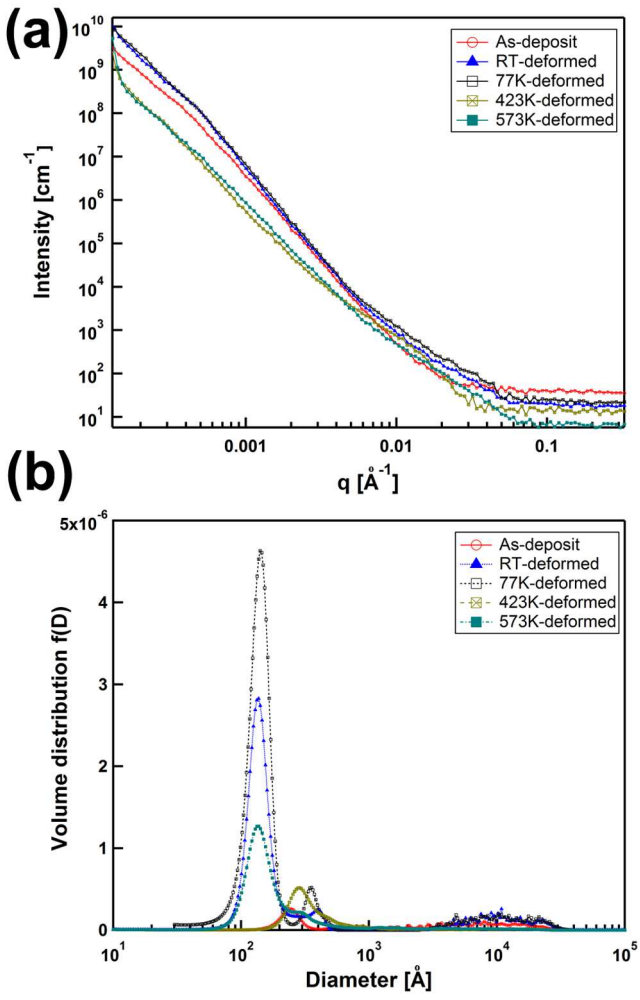

Figure 10 BF11812 30NOV2011

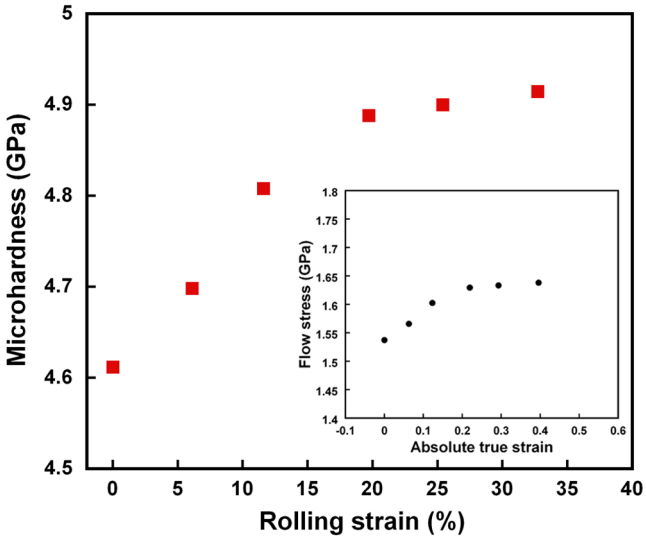

Figure 11 BF11812 30NOV2011

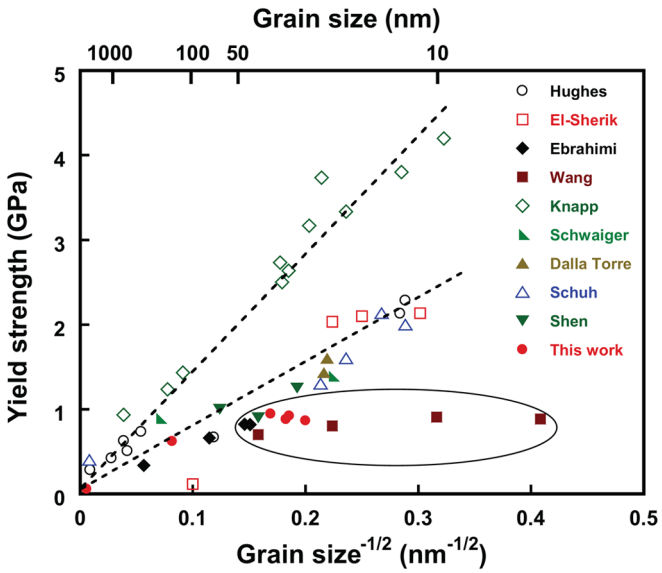

Figure 12 BF11812 30NOV2011

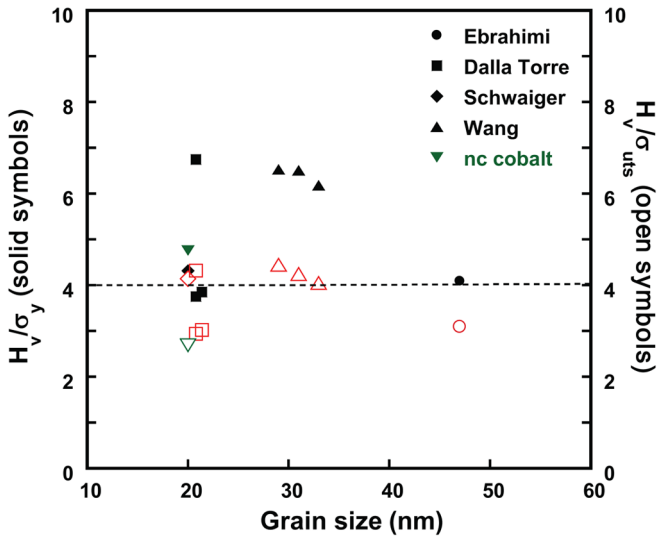

Figure 13 BF11812 30NOV2011

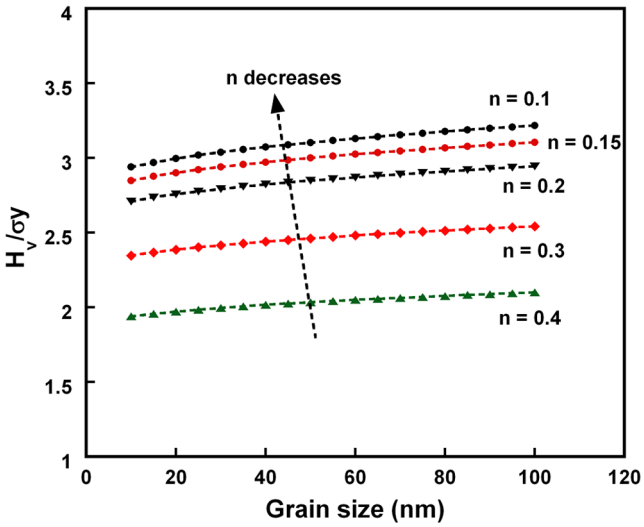

Figure 14 BF11812 30NOV2011

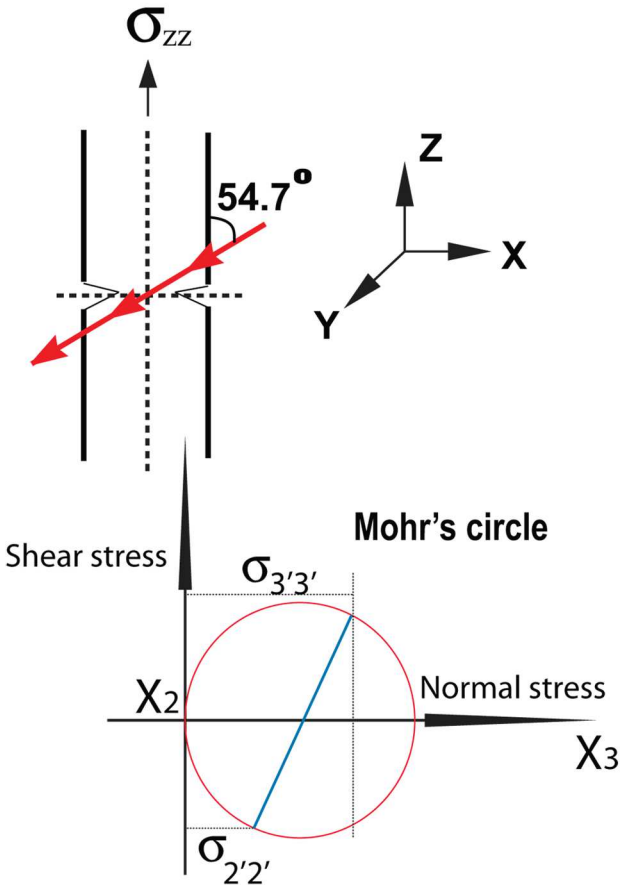

Figure 15 BF11812 30NOV2011